

## **Distribution Agreement**

In presenting this thesis or dissertation as a partial fulfillment of the requirements for an advanced degree from Emory University, I hereby grant to Emory University and its agents the non-exclusive license to archive, make accessible, and display my thesis or dissertation in whole or in part in all forms of media, now or hereafter known, including display on the world wide web. I understand that I may select some access restrictions as part of the online submission of this thesis or dissertation. I retain all ownership rights to the copyright of the thesis or dissertation. I also retain the right to use in future works (such as articles or books) all or part of this thesis or dissertation.

Signature:

---

Megan Rachelle Hockman

---

Date

Reassortment of Mammalian Orthoreovirus

By

Megan Rachelle Hockman  
Doctor of Philosophy

Graduate Division of Biological and Biomedical Science

Microbiology and Molecular Genetics

---

Anice C. Lowen  
Advisor

---

Victor Faundez  
Committee Member

---

Katharina V. Koelle  
Committee Member

---

Bernardo A. Mainou  
Committee Member

---

David Steinhauer  
Committee Member

Accepted:

---

Kimberly Jacob Arriola, Ph.D., MPH  
Dean of the James T. Laney School of Graduate Studies

---

Date

Reassortment of Mammalian Orthoreovirus

By

Megan Rachelle Hockman  
B.S., Duquesne University, 2016

Advisor: Anice C. Lowen, Ph.D.

An abstract of  
A dissertation submitted to the Faculty of the  
James T. Laney School of Graduate Studies of Emory University  
in partial fulfillment of the requirements for the degree of  
Doctor of Philosophy in  
Graduate Division of Biological and Biomedical Science  
Microbiology and Molecular Genetics  
2021

## Abstract

### Reassortment of Mammalian Orthoreovirus

By Megan Rachelle Hockman

Viral evolution can facilitate the generation of viral variants that escape therapeutics, subvert vaccination, and enter the human population from other host species. Studies of viral evolution therefore provide mechanistic insight into variant emergence. One potential driver of evolution relevant for segmented viruses is reassortment. During cellular co-infection, the segments of co-infecting viruses can mix and may be co-packaged. This results in progeny bearing novel combinations of the parental genes, a potentially important source of genetic diversity. The degree to which the virus' replication mechanism impacts its ability to undergo reassortment is an area of ongoing research. Mammalian orthoreovirus (reovirus) represents an interesting system in which to study the relationship between replication mechanism and reassortment frequency. Viral inclusion bodies, which house replication machinery and viral mRNA, are hypothesized to impose a physical barrier to the mixing of parental mRNAs. Two commonly studied serotypes of reovirus, T1L and T3D, are known to generate inclusions with filamentous and globular morphologies, respectively. A single amino acid is responsible for this difference, allowing for the generation of inclusion mutants within the same serotype and the subsequent investigation of the impact of inclusion morphology on reassortment frequency. Reassortment studies were performed using an unbiased system. We developed this system to enable quantification of reassortment in the absence of protein or nucleic acid mismatch and quantified T1L and T3D reassortment using this system. Data were then compared to a mathematical model which assumed free segment mixing. We found that T3D reassortment occurs with comparable frequency to that predicted by the model, and T1L reassortment occurs less frequently. Alteration of inclusion body morphology in each serotype did not impact reassortment efficiency. Furthermore, blocking of inclusion body merging using the microtubule depolymerizing agent nocodazole did not impact reassortment frequency. We have developed a system in which to quantify reovirus reassortment. Using this system, we have concluded that inclusion morphology is not a determinant of reassortment frequency, and that inclusion coalescence is not a requirement for genetic exchange.

Reassortment of Mammalian Orthoreovirus

By

Megan Rachelle Hockman  
B.S., Duquesne University, 2016

Advisor: Anice C. Lowen, Ph.D.

A dissertation submitted to the Faculty of the  
James T. Laney School of Graduate Studies of Emory University  
in partial fulfillment of the requirements for the degree of  
Doctor of Philosophy  
in  
Graduate Division of Biological and Biomedical Science  
Microbiology and Molecular Genetics  
2021

## **Acknowledgments**

I would first like to sincerely thank Anice Lowen for her incredible mentorship throughout my years at Emory. She has been an incredible example of what it means to be an excellent scientist and mentor, and I am extremely grateful that she took me under her wing.

Second, I'd like to thank the current and past members of the Lowen lab: Kate Holmes, Gabrielle Delima, Jessica Shartouny, Meher Sethi, Maria White, Nate Jacobs, Kara Phipps, Ketaki Ganti, Chung-Young Lee, Camden Bair, Dave VanInsberghe, Lucas Ferreri, Lisa Bono, Courtney Steger, Hui Tao, and Shamika Danzy-Bedoya. All have provided conversation, advice, reagents, friendship, and countless hours of their time, and for that I can't thank them enough.

My friends, who were there to listen to my talks (even though they had no idea what I was saying), give advice, hype me up, and ignore all my rolls below 10. Sam Cummings, Andrew Anderson, Olivia Bjerk, Zach Dison, Tyler Lawson, and Tim Kimbrough.

My family away from home: Colin, Corin, and Felix Egelhoff. Thank you for being there for all the moments I stepped away from the lab, and for all the moments I brought the lab with me into real life.

My running family: Zac and Jen Raby, who got me on the trails so I could learn that ultramarathons and a PhD are really just two sides of the same coin. And for all of the snacks.

Jeff, for his patience, love, and encouragement.

Pip, for snuggles, unending love, and being the only thing I can stand to wake up for at 5am.

My parents, Eric and Carey, for their unwavering love and support, incredible food, and reminding me that balance is always key.

## **Table of Contents**

**Abstract**

**Acknowledgments**

**Table of Contents**

**List of Figures and Tables**

**Author Contributions**

**Chapter I. Introduction..... 1**

Introduction ..... 1

References .....10

**Chapter II. A method for the unbiased quantification of reassortment in segmented viruses ..... 16**

Abstract ..... 17

Introduction ..... 17

Results ..... 20

Discussion ..... 24

Materials and Methods ..... 27

Acknowledgements ..... 35

Figures and tables ..... 36

References ..... 47

**Chapter III. Mammalian orthoreovirus reassortment proceeds with little constraint on segment mixing..... 51**

Abstract ..... 52

Introduction ..... 53

Results ..... 55

Discussion ..... 61

Materials and Methods ..... 64

Acknowledgments ..... 70

Figures and Tables ..... 71

References ..... 78

**Chapter IV. Summary ..... 82**

Summary ..... 82  
References ..... 91

## **List of Figures and Tables**

<b>Chapter II. A method for the unbiased quantification of reassortment in segmented viruses</b> .....	Error! Bookmark not defined.
<b>Figure 1.</b> <i>Design of variant mutations</i> .....	36
<b>Figure 2.</b> <i>Example 384-well plate layouts for high-resolution melt analysis</i> .....	37
<b>Figure 3.</b> <i>Single nucleotide changes do not detectably alter variant virus growth</i> .....	38
<b>Figure 4.</b> <i>Flow cytometry allows for the quantification of infected and co-infected cells in a population</i> .....	39
<b>Figure 5.</b> <i>Melt curves allow the determination of parental segment origin</i> .....	40
<b>Figure 6.</b> <i>Reassortment tables provide visual representation of progeny virus genotypes</i> .	41
<b>Figure 7.</b> <i>Comparison of IAV infection levels and reassortment</i> .....	42
<b>Table 1.</b> <i>Point mutations used to generate variant viruses</i> .....	43
<b>Table 2.</b> <i>Primers used to generate amplicons for high-resolution melt analysis</i> .....	44
<b>Table 3.</b> <i>Expected % co-infection from Poisson statistics</i> .....	46
<b>Chapter III. Mammalian orthoreovirus reassortment proceeds with little constraint on segment mixing</b> .....	Error! Bookmark not defined.
<b>Figure 1.</b> <i>T1L co-infection partners grow to equivalent titers and can be differentiated using high resolution melt analysis</i> .....	71
<b>Figure 2.</b> <i>Reovirus reassortment occurs frequently at high MOI and is more efficient in T3D than in T1L</i> .....	72
<b>Figure 3.</b> <i>Under high MOI conditions, there is little pairwise association between gene segments</i> .....	73
<b>Figure 4.</b> <i>Reassortment efficiency is impacted by inclusion morphology in T3D but not T1L</i> .....	74
<b>Figure 5.</b> <i>Flow cytometry-based detection of reovirus-positive cells appears to under-represent levels of infection</i> .....	76
<b>Figure 6.</b> <i>Blocking inclusion merging with nocodazole does not impact reassortment</i> .....	77

## **Authorship Contributions**

I first-authored the publication in chapter two, which was published in the *Journal of Virological Methods* in 2020. My contributions included experiments leading to the data in Figures 3, 4, 5, and 6. I designed, generated, and characterized mammalian orthoreovirus *var* mutants. I chose the *var* mutation sites, generated plasmids for reverse genetics of *var* viruses, and grew virus stocks of both *wt* and *var* reovirus. I then performed single-cycle growth experiments, co-infections, and genotype analysis of mammalian orthoreovirus, which were my contributions to this work. I performed data analysis for the reovirus sections of Figures 3, 4, 5, and 6, and designed original forms of all the figures. I wrote the original draft of the entire manuscript and participated in editing and review of the final draft.

I am the first author on the manuscript in chapter three. I contributed to project development, experimental design, data collection, interpretation, and analysis. I characterized growth of T1L viruses, performed co-infections for subsequent reassortment analysis, and I was responsible for generation of the reassortment tables that lead to Figures 2, 4, and 6, and plotted all the data therein. I obtained the confocal microscopy images in figures 4 and 6, as well as the infection and output data in figure 5. Nathan Jacobs wrote the code to obtain figure 3, and provided assistance with the methods and results sections related to that figure. I wrote the original draft of the manuscript and edited the subsequent drafts with the assistance of the co-authors.

## Chapter I. Introduction

### Introduction

Viral evolution places a significant burden on public health by causing the subversion of existing vaccines and antivirals and driving the emergence of novel pathogens. These novel pathogens may have enhanced morbidity and mortality, increasing the burden of disease on the population. Viruses may also evolve to infect new hosts, crossing from non-human animals to humans and necessitating the creation of new vaccines or antivirals. Viruses for which vaccines already exist may continue to evolve, rendering previously administered vaccines ineffective. Critical gaps in treatment occur when viruses evolve to subvert existing therapeutic measures. Outbreaks resulting from viral evolution can cause significant loss of human life, social disruption, reductions in productivity, and necessitate costly treatment of patients. Understanding the mechanisms underlying viral evolution is a critical first step in the development of effective strategies to limit the impact of viral diseases.

#### *Mammalian orthoreovirus life cycle*

Outside of cells, mammalian orthoreovirus exists as a double-layered particle with two proteinaceous capsid layers that house its segmented dsRNA genome (1). The outer capsid is composed of heterohexameric complexes of the  $\mu_1$  and  $\sigma_3$  proteins (1). This outer capsid encapsulates an inner capsid composed of the  $\sigma_2$  protein and the  $\lambda_1$  protein, which anchors the  $\lambda_3$  polymerase subunits at the five-fold axes of symmetry. The  $\lambda_3$  polymerase has additional interactions with the  $\mu_2$  polymerase co-factor. The five-fold axes of symmetry of these layers are perforated by the capping enzyme and core spike protein ( $\lambda_2$ ) and the receptor-binding spike protein ( $\sigma_1$ ) (1). Prior to receptor binding, which triggers endocytosis, the  $\sigma_1$  spike protein binds to sialic acid residues on the cell surface. This binding is a key determinant of tissue tropism *in vivo* and differs between the T1L and T3D serotypes. The  $\sigma_1$  protein then binds to host cell

receptor junction adhesion molecule-A (JAM-A) (2). This binding triggers receptor-mediated endocytosis, after which the virus is sorted into a host cell endosome (3, 4).

Within the endosomes, the virion is cleaved by host cell proteases into discrete intermediates, the first of which is termed the infectious sub-virion particle (ISVP) (1, 5, 6). The ISVP is formed when outer capsid structural protein  $\sigma_3$  is cleaved by cysteine proteases and removed. The spike protein  $\sigma_1$  undergoes a conformational change during conversion to an ISVP, and the  $\mu_1$  protein is also proteolytically cleaved (1, 4). Proteolysis is performed by cathepsin L and B proteases in fibroblasts (6) and can be inhibited by addition of protease inhibitor E65 or addition of  $\text{NH}_4\text{Cl}$  which prevents acidification of endosomes (5-7). Conformational changes in  $\mu_1$  and loss of the  $\sigma_1$  protein characterize formation of the ISVP\*, the second disassembly intermediate (1, 4).  $\mu_1\text{N}$ , a cleavage product of  $\mu_1$ , is responsible for the formation of pores in the endosomal membrane through which core particles are extruded (1, 4, 8, 9).

Reovirus infection induces the formation of stress granules (10, 11). Stress granules are liquid-liquid phase separated compartments that form in response to cellular stress, sequestering stalled ribosomal complexes until the stress has passed, at which point they dissipate and release their contents so cellular translation can proceed (12). Viral core particles localize to stress granules early in infection, after their exit from endosomes (10). It is hypothesized these may serve as early vessels in which to sequester viral replication, until inclusion bodies are formed. When stress granules dissipate, viral core particles proceed to localize to inclusion bodies, where they remain for the duration of the viral life cycle (10, 13, 14).

Virus core particles become transcriptionally active upon the removal of the  $\sigma_1$  protein from the polymerase complexes during endocytosis (1). Reovirus mRNAs, which possess a 5' cap but not a 3' poly(A) tail, are produced by transcriptionally active core particles, which contain polymerase and capping enzymes that exist as turrets at the five-fold axes of symmetry (15-17).

Evidence suggests there is some level of temporal control to this process, as mRNAs are found in different abundances throughout the virus life cycle (17). mRNAs are translated to proteins by cellular ribosomes. Active protein translation can occur within stress granules (18), and reovirus may utilize these as precursors to inclusion bodies that serve to concentrate virus replication machinery early in infection (11). Later in the infection process, ribosomes localize to the periphery of inclusion bodies (11, 19).

Relatively little is known about the viral assembly and egress pathway. Interactions between segments that facilitate co-packaging are hypothesized to be important components in the assembly of bluetongue virus, a member of the *Reoviridae* family (20). Limited data are available on the precise mechanism of genome packaging utilized by reovirus (21), but evidence suggests the existence of packaging signals at both the 3' and 5' ends of positive stranded RNAs (22-25). It is possible that interactions between segments are specific and mediate co-packaging. Whether assembly occurs in a concerted or sequential manner is not known. Electron microscopy has shown empty viral cores within inclusion bodies (14, 26) which may either represent assembly intermediates or dead-end products. The latter interpretation is favored due to RNA-RNA interactions, which would produce a concatemer that is not conducive to a sequential packaging mechanism akin to that of dsRNA phages (21, 27). Concatemers of RNA are expected to be packaged in a concerted manner, with capsid layers assembling around them. Empty cores would be unable to accept a genome and are therefore dead-end products.

The viral assembly mechanism and egress pathway are ongoing areas of research, with very little understood. The steps that lead to the formation of the inner capsid, complete with genome and enzymes, are not known. The outer capsid is composed of  $\sigma 3$  and  $\mu 1$  proteins (28). Purified  $\sigma 3$ , with the aid of the cellular tailless complex polypeptide 1 ring complex (TRiC) chaperonin, can coat ISVPs to form a mature virus particle (29, 30). This may be the mechanism by which mature virions are formed prior to egress. New evidence has revealed that reovirus

uses a novel, non-lytic egress pathway that involves modified lysosomal membranes that transport mature virions to the cell surface where they are released, but lytic egress remains a possibility (31, 32). The details of this pathway, such as how mature virions are recruited into these vesicles, are areas of ongoing study.

### *Inclusion bodies*

Inclusion bodies (inclusions), or viral factories, are generated by many virus families. Some co-opt host cell membranes to enclose their replication machinery (33). Reovirus inclusions, however, are complex proteinaceous structures that are not membrane-bound. Only one such protein,  $\mu$ NS, is necessary for formation of inclusion-like bodies. Expression of this protein alone results in the formation of globular inclusion-like structures within the cytoplasm (34, 35). There are several domains in the  $\mu$ NS protein that interact with other viral proteins and may serve to localize them to inclusion bodies during replication (13, 36, 37). Short regions of  $\mu$ NS interact with viral core particles, resulting in recruitment of cores to inclusion bodies and localization of mRNA synthesis (37). Residues 1 to 40 are sufficient for  $\mu$ NS association with both  $\sigma$ NS, an RNA binding protein (36), and  $\mu$ 2, which has been shown to be the determinant of inclusion body morphology (38).

Expression of both  $\mu$ 2 and  $\mu$ NS in cells results in the adoption of characteristic inclusion morphologies, which are dictated by  $\mu$ 2 amino acid 208 (38). A proline at this position causes inclusions to take on a filamentous morphology, which is observed in most reovirus serotypes. This morphology is dictated by the stability of the microtubule network, as microtubules are utilized as a scaffolding for inclusions. Mutation of this proline to a serine abrogates the association of inclusions with microtubules, resulting in a globular morphology. This mutation additionally causes frequent misfolding, ubiquitination, and aggregation of the  $\mu$ 2 protein (39). Aside from impacting inclusion body morphology,  $\mu$ 2 amino acid 208 is a determinant of IFN- $\beta$  repression by reovirus (40).

Viral inclusions are observed starting around 4 hours post infection, when sufficient levels of  $\mu$ NS are expressed. These early inclusion bodies are small and dispersed throughout the cytoplasm. As infection progresses, inclusions begin to take on characteristic morphologies and move towards the perinuclear region. Live cell imaging has shown inclusion dynamics which are hypothesized to be stochastic (41). When small inclusions come into contact with one another, they coalesce to form larger structures (41, 42). This is evidenced by a reduction in the overall number of inclusions but an increase of inclusion area over time (42). Addition of a microtubule depolymerizing agent, nocodazole, makes inclusions incapable of merging. Images show small inclusions moving through the cytoplasm, coming into contact, but then moving away from each other without merging (41). The mechanism by which nocodazole blocks inclusion merging is not understood, but this phenotype persists in both globular and filamentous viruses.

Ribosomal subunits and translational factors used in initiation and elongation localize to viral inclusions. Components of the 43S preinitiation complex colocalize with  $\sigma$ NS at the periphery of inclusions, suggesting recruitment of ribosomes by  $\sigma$ NS (43). Furthermore, fragments of endoplasmic reticulum membrane along with ribosomes were seen within inclusion bodies using electron microscopy (19, 44, 45). This may serve to localize the translation step of the viral replication cycle, meaning viral mRNAs do not have to traffic to the cytoplasm to be translated. Few published examples of reovirus mRNA visualization exist, but they show that newly transcribed mRNAs localize to inclusion bodies (37, 45).

With respect to reassortment, inclusion bodies present a potential barrier to genetic exchange. Sequestration of mRNAs within inclusions of parental virus origin would limit reassortment. However, inclusion coalescence may provide a mechanism to facilitate genetic exchange. The impacts of inclusion morphology and coalescence on reassortment are covered in Chapter III of this dissertation.

*Reassortment and evolution*

The introduction of point mutations is a major source of genetic variation that occurs across virus families at variable rates, more frequently in RNA viruses than DNA viruses. Quantification of mutation in substitutions per nucleotide per cell infection (s/n/c) shows rates of  $10^{-6} - 10^{-8}$  s/n/c in DNA viruses and  $10^{-4} - 10^{-6}$  s/n/c in RNA viruses due to differences in polymerase fidelity (46-48). Another source of diversity, molecular recombination, has been shown to occur in both DNA and RNA viruses, such as herpesviruses and poliovirus (49-51). This type of recombination involves polymerase template switching between nucleic acid strands from different parental viruses to yield chimeric genomes. Genome segmentation is present in virus families such as *Arenaviridae*, *Bunyaviridae*, *Orthomyxoviridae*, and *Reoviridae*. Viruses in these families contain multiple genome segments which can be exchanged in their entirety when multiple viruses infect the same cell, a type of recombination termed reassortment. The resultant progeny bear a mix of both parental segments. Influenza A virus reassorts frequently, in part due to the prevalence of incomplete viral genomes (52-54). A virion which either does not contain or does not replicate a full complement of segments within a host cell will fail to establish a productive infection. In this case, a full complement of segments may be provided by multiple co-infecting viruses. Progeny that arise from these co-infections are reassortant, bearing segments from the co-infecting parental viruses. High prevalence of incomplete genomes is one source of the observed high levels of influenza A virus reassortment. This is one example of how a virus' life cycle can impact the frequency at which it reassorts. The reassortment frequency and underlying replication mechanisms remain understudied in many systems, such as that of mammalian orthoreovirus. Reovirus is a segmented virus which has been demonstrated to undergo reassortment (55-58), but the presence and frequency of incomplete genomes in reovirus has not been determined. A comprehensive quantification of its reassortment potential is also lacking. We hypothesize that inclusion bodies that serve to focus the virus' life cycle to discrete locations within the cytoplasm present a potential barrier to

reassortment. The degree to which a virus' life cycle impacts its ability to reassort may yield important insights into the prevalence of reassortment as an evolutionary mechanism.

The prevalence of reassortment in segmented viruses is an area of ongoing interest in the field of virus evolution. Studies in the bacteriophage  $\phi 6$  have revealed that reassortment is similar to sex in viruses in that it alleviates the effects of Muller's ratchet: the accumulation of deleterious mutants in the absence of recombination or sex (59, 60). In the absence of reassortment or recombination, deleterious mutations can accumulate resulting in a reduction in population fitness. The high mutation rates in RNA viruses increase the likelihood of deleterious mutations, so asexual virus populations may be particularly susceptible to Muller's ratchet. Reassortment and genetic recombination can result in the loss of these deleterious mutations, provided that multiple variants exist within a population. A very small bottleneck may permit Muller's ratchet to persist, as it limits the number of variants in the population and therefore the likelihood of recombination providing a beneficial allele (61).

Reassortment may also facilitate the combining of beneficial mutations, resulting in viruses with enhanced fitness, host range, or immune avoidance mechanisms. This phenomenon has been documented in influenza virus (62-64), and reovirus interspecies transmission has been facilitated by reassortment events (65, 66). While documented cases of reassortment in reovirus exist (55, 57, 58, 65-67), it remains unknown how likely this phenomenon is to occur at the cellular level.

Reassortment in reovirus was previously studied using temperature-sensitive (ts) mutants. These experiments yielded low frequencies of reassortment, between 3-8% depending on co-infection pairs and multiplicity of infection (55-57, 67). Using these values, we extrapolated that reassortment of any of the ten genome segments leads to an estimation of 6-16% reassortment overall. Other experiments studied reassortment between the T1L and T3D serotypes (58). This allowed for quantification of reassortment of all segments but may have had

limitations imposed by mismatched parental viruses. Progeny resulting from co-infections with different parental serotypes may have impaired fitness due to nucleic acid or protein mismatch. Incompatibilities in nucleic acids may result in an inability for them to be co-packaged, while mismatched proteins may not function properly together, resulting in attenuation. In these cases, reassortant progeny would be underrepresented in the subsequent analysis. The development of reovirus reverse genetics (68), as well as streamlined assays for viral genotyping (69, 70), make it possible to quantify reassortment between matched parental viruses. In the first study, detailed in Chapter II, we sought to use these advances to develop an unbiased system in which to quantify reovirus reassortment. This system introduces a single silent point mutation into each wild-type (*wt*) virus genome segment, yielding a variant (*var*) virus. These highly similar virus pairs are used in co-infections, and the parental origin of each segment can be identified using PCR-based approaches. The high degree of similarity between parental viruses allows reassortment to occur in the absence of mismatch. Thus, the *wt* and *var* viruses can be used to co-infect cells, and reassortment frequency in the absence of barriers imposed by segment mismatch can be determined based on progeny genotypes. The details of this method can be found in Chapter II of this dissertation.

### *Introduction to thesis project*

The goal of this project was to quantify the reassortment of mammalian orthoreovirus, and to investigate the role of inclusion bodies in modulating reassortment frequency. These studies give important insights into the prevalence of reassortment in reovirus, the potential impact of inclusion-based replication on genetic exchange and provide quantitative evidence of reassortment potential in reovirus.

The first aim of this research was to develop a system in which reassortment could be quantified in the absence of selection. The presence of such mismatches may result in an inability of segments to be packaged together, or reduced fitness of reassortant progeny due to

protein incompatibilities. To avoid such pitfalls, we used silent point mutations as genetic markers for the identification of parental segment origin. Methodological details and results can be found in Chapter II of this dissertation.

The second aim of this research was to use the developed system to investigate reovirus reassortment frequency. Comparison of different serotypes suggests that T3D reassorts more efficiently than T1L. Further studies on the role of inclusion morphology and coalescence indicated that inclusions do not play a major role in dictating reovirus reassortment potential. Experimental details can be found in Chapter III.

Overall, the thesis work detailed herein provides novel quantification of reovirus reassortment, revealing that barriers within the cell do not appreciably limit reovirus reassortment. This ample opportunity for genetic exchange within co-infected cells may allow for reovirus to take advantage of the evolutionary benefits of reassortment. On the surface, reovirus inclusions and its replicative cycle appear to be potentially strong inhibitors of reassortment. The development of replication features that limit reassortment would have provided compelling evidence that perhaps reassortment is not a necessary process with which all segmented viruses generate diversity. That is, genome segmentation does not guarantee reassortment, and viruses such as reovirus do not take advantage of its potential benefits. However, the data we have collected suggest that even in systems which appear to limit reassortment, the process is still efficient. Genetic exchange may be more prevalent in segmented viruses than previously hypothesized, allowing diversification in multiple segmented virus families and potentially indicating an evolutionary advantage of reassortment.

## References

1. Knipe DM, Howley PM. 2013. *Fields virology*, 6th ed. Wolters Kluwer/Lippincott Williams & Wilkins Health, Philadelphia, PA.
2. Koehler M, Aravamudhan P, Guzman-Cardozo C, Dumitru AC, Yang J, Gargiulo S, Soumillion P, Dermody TS, Alsteens D. 2019. Glycan-mediated enhancement of reovirus receptor binding. *Nat Commun* 10:4460.
3. Koehler M, Petitjean SJL, Yang J, Aravamudhan P, Somoulay X, Lo Giudice C, Poncin MA, Dumitru AC, Dermody TS, Alsteens D. 2021. Reovirus directly engages integrin to recruit clathrin for entry into host cells. *Nat Commun* 12:2149.
4. Mainou BA. 2017. The Orchestra of Reovirus Cell Entry. *Curr Clin Microbiol Rep* 4:142-149.
5. Doyle JD, Danthi P, Kendall EA, Ooms LS, Wetzel JD, Dermody TS. 2012. Molecular determinants of proteolytic disassembly of the reovirus outer capsid. *J Biol Chem* 287:8029-38.
6. Ebert DH, Deussing J, Peters C, Dermody TS. 2002. Cathepsin L and cathepsin B mediate reovirus disassembly in murine fibroblast cells. *J Biol Chem* 277:24609-17.
7. Sturzenbecker LJ, Nibert M, Furlong D, Fields BN. 1987. Intracellular digestion of reovirus particles requires a low pH and is an essential step in the viral infectious cycle. *J Virol* 61:2351-61.
8. Agosto MA, Ivanovic T, Nibert ML. 2006. Mammalian reovirus, a nonfusogenic nonenveloped virus, forms size-selective pores in a model membrane. *Proc Natl Acad Sci U S A* 103:16496-501.
9. Ivanovic T, Agosto MA, Zhang L, Chandran K, Harrison SC, Nibert ML. 2008. Peptides released from reovirus outer capsid form membrane pores that recruit virus particles. *EMBO J* 27:1289-98.
10. Qin Q, Hastings C, Miller CL. 2009. Mammalian orthoreovirus particles induce and are recruited into stress granules at early times postinfection. *J Virol* 83:11090-101.
11. Guo Y, Parker JSL. 2021. The Paradoxes of Viral mRNA Translation during Mammalian Orthoreovirus Infection. *Viruses* 13.
12. Ivanov P, Kedersha N, Anderson P. 2019. Stress Granules and Processing Bodies in Translational Control. *Cold Spring Harb Perspect Biol* 11.
13. Broering TJ, Kim J, Miller CL, Piggott CD, Dinoso JB, Nibert ML, Parker JS. 2004. Reovirus nonstructural protein mu NS recruits viral core surface proteins and entering core particles to factory-like inclusions. *J Virol* 78:1882-92.

14. Shah PNM, Stanifer ML, Hohn K, Engel U, Haselmann U, Bartenschlager R, Krausslich HG, Krijnse-Locker J, Boulant S. 2017. Genome packaging of reovirus is mediated by the scaffolding property of the microtubule network. *Cell Microbiol* 19.
15. Yeager M, Weiner S, Coombs K. Transcriptionally active reovirus core particles visualized by electron cryo-microscopy and image reconstruction, p SU484-SU484. *In* (ed), CELL PRESS 50 HAMPSHIRE ST, FLOOR 5, CAMBRIDGE, MA 02139 USA,
16. Reinisch KM, Nibert ML, Harrison SC. 2000. Structure of the reovirus core at 3.6 Å resolution. *Nature* 404:960-7.
17. Nonoyama M, Millward S, Graham AF. 1974. Control of transcription of the reovirus genome. *Nucleic Acids Res* 1:373-85.
18. Mateju D, Eichenberger B, Voigt F, Eglinger J, Roth G, Chao JA. 2020. Single-Molecule Imaging Reveals Translation of mRNAs Localized to Stress Granules. *Cell* 183:1801-1812 e13.
19. Desmet EA, Anguish LJ, Parker JS. 2014. Virus-mediated compartmentalization of the host translational machinery. *mBio* 5:e01463-14.
20. Sung PY, Roy P. 2014. Sequential packaging of RNA genomic segments during the assembly of Bluetongue virus. *Nucleic Acids Res* 42:13824-38.
21. Borodavka A, Desselberger U, Patton JT. 2018. Genome packaging in multi-segmented dsRNA viruses: distinct mechanisms with similar outcomes. *Curr Opin Virol* 33:106-112.
22. Roner MR, Bassett K, Roehr J. 2004. Identification of the 5' sequences required for incorporation of an engineered ssRNA into the Reovirus genome. *Virology* 329:348-60.
23. Roner MR, Lin PN, Nepluev I, Kong LJ, Joklik WK. 1995. Identification of signals required for the insertion of heterologous genome segments into the reovirus genome. *Proc Natl Acad Sci U S A* 92:12362-6.
24. Roner MR, Roehr J. 2006. The 3' sequences required for incorporation of an engineered ssRNA into the Reovirus genome. *Virol J* 3:1.
25. Roner MR, Steele BG. 2007. Localizing the reovirus packaging signals using an engineered m1 and s2 ssRNA. *Virology* 358:89-97.
26. Sutton G, Sun D, Fu X, Kotecha A, Hecksel CW, Clare DK, Zhang P, Stuart DI, Boyce M. 2020. Assembly intermediates of orthoreovirus captured in the cell. *Nat Commun* 11:4445.
27. Qiao X, Qiao J, Mindich L. 1997. Stoichiometric packaging of the three genomic segments of double-stranded RNA bacteriophage phi6. *Proc Natl Acad Sci U S A* 94:4074-9.
28. Dryden KA, Wang G, Yeager M, Nibert ML, Coombs KM, Furlong DB, Fields BN, Baker TS. 1993. Early steps in reovirus infection are associated with dramatic changes in

- supramolecular structure and protein conformation: analysis of virions and subviral particles by cryoelectron microscopy and image reconstruction. *J Cell Biol* 122:1023-41.
29. Knowlton JJ, Gestaut D, Ma B, Taylor G, Seven AB, Leitner A, Wilson GJ, Shanker S, Yates NA, Prasad BVV, Aebersold R, Chiu W, Frydman J, Dermody TS. 2021. Structural and functional dissection of reovirus capsid folding and assembly by the prefoldin-TRiC/CCT chaperone network. *Proc Natl Acad Sci U S A* 118.
  30. Knowlton JJ, Fernandez de Castro I, Ashbrook AW, Gestaut DR, Zamora PF, Bauer JA, Forrest JC, Frydman J, Risco C, Dermody TS. 2018. The TRiC chaperonin controls reovirus replication through outer-capsid folding. *Nat Microbiol* 3:481-493.
  31. de Castro IF, Fernandez JJ, Dermody TS, Risco C. 2021. Electron Tomography to Study the Three-dimensional Structure of the Reovirus Egress Pathway in Mammalian Cells. *Bio Protoc* 11:e4080.
  32. Fernandez de Castro I, Tenorio R, Ortega-Gonzalez P, Knowlton JJ, Zamora PF, Lee CH, Fernandez JJ, Dermody TS, Risco C. 2020. A modified lysosomal organelle mediates nonlytic egress of reovirus. *J Cell Biol* 219.
  33. Hsu NY, Ilnytska O, Belov G, Santiana M, Chen YH, Takvorian PM, Pau C, van der Schaar H, Kaushik-Basu N, Balla T, Cameron CE, Ehrenfeld E, van Kuppeveld FJ, Altan-Bonnet N. 2010. Viral reorganization of the secretory pathway generates distinct organelles for RNA replication. *Cell* 141:799-811.
  34. Becker MM, Peters TR, Dermody TS. 2003. Reovirus sigma NS and mu NS proteins form cytoplasmic inclusion structures in the absence of viral infection. *J Virol* 77:5948-63.
  35. Broering TJ, Parker JS, Joyce PL, Kim J, Nibert ML. 2002. Mammalian reovirus nonstructural protein microNS forms large inclusions and colocalizes with reovirus microtubule-associated protein micro2 in transfected cells. *J Virol* 76:8285-97.
  36. Miller CL, Broering TJ, Parker JS, Arnold MM, Nibert ML. 2003. Reovirus sigma NS protein localizes to inclusions through an association requiring the mu NS amino terminus. *J Virol* 77:4566-76.
  37. Miller CL, Arnold MM, Broering TJ, Hastings CE, Nibert ML. 2010. Localization of mammalian orthoreovirus proteins to cytoplasmic factory-like structures via nonoverlapping regions of microNS. *J Virol* 84:867-82.
  38. Parker JS, Broering TJ, Kim J, Higgins DE, Nibert ML. 2002. Reovirus core protein mu2 determines the filamentous morphology of viral inclusion bodies by interacting with and stabilizing microtubules. *J Virol* 76:4483-96.
  39. Miller CL, Parker JS, Dinoso JB, Piggott CD, Perron MJ, Nibert ML. 2004. Increased ubiquitination and other covariant phenotypes attributed to a strain- and temperature-dependent defect of reovirus core protein mu2. *J Virol* 78:10291-302.
  40. Irvin SC, Zurney J, Ooms LS, Chappell JD, Dermody TS, Sherry B. 2012. A single-amino-acid polymorphism in reovirus protein mu2 determines repression of interferon signaling and modulates myocarditis. *J Virol* 86:2302-11.

41. Bussiere LD, Choudhury P, Bellaire B, Miller CL. 2017. Characterization of a Replicating Mammalian Orthoreovirus with Tetracysteine-Tagged muNS for Live-Cell Visualization of Viral Factories. *J Virol* 91.
42. Eichwald C, Ackermann M, Nibert ML. 2018. The dynamics of both filamentous and globular mammalian reovirus viral factories rely on the microtubule network. *Virology* 518:77-86.
43. Huismans H, Joklik WK. 1976. Reovirus-coded polypeptides in infected cells: isolation of two native monomeric polypeptides with affinity for single-stranded and double-stranded RNA, respectively. *Virology* 70:411-24.
44. Fernandez de Castro I, Zamora PF, Ooms L, Fernandez JJ, Lai CM, Mainou BA, Dermody TS, Risco C. 2014. Reovirus forms neo-organelles for progeny particle assembly within reorganized cell membranes. *mBio* 5.
45. Tenorio R, Fernandez de Castro I, Knowlton JJ, Zamora PF, Lee CH, Mainou BA, Dermody TS, Risco C. 2018. Reovirus sigmaNS and muNS Proteins Remodel the Endoplasmic Reticulum to Build Replication Neo-Organelles. *mBio* 9.
46. Duffy S, Shackelton LA, Holmes EC. 2008. Rates of evolutionary change in viruses: patterns and determinants. *Nat Rev Genet* 9:267-76.
47. Sanjuan R, Nebot MR, Chirico N, Mansky LM, Belshaw R. 2010. Viral mutation rates. *J Virol* 84:9733-48.
48. Simon-Loriere E, Holmes EC. 2011. Why do RNA viruses recombine? *Nat Rev Microbiol* 9:617-26.
49. Perez-Losada M, Arenas M, Galan JC, Palero F, Gonzalez-Candelas F. 2015. Recombination in viruses: mechanisms, methods of study, and evolutionary consequences. *Infect Genet Evol* 30:296-307.
50. Hirst GK. 1962. Genetic recombination with Newcastle disease virus, polioviruses, and influenza. *Cold Spring Harb Symp Quant Biol* 27:303-9.
51. Ledinko N. 1963. Genetic recombination with poliovirus type 1. Studies of crosses between a normal horse serum-resistant mutant and several guanidine-resistant mutants of the same strain. *Virology* 20:107-19.
52. Fonville JM, Marshall N, Tao H, Steel J, Lowen AC. 2015. Influenza Virus Reassortment Is Enhanced by Semi-infectious Particles but Can Be Suppressed by Defective Interfering Particles. *PLoS Pathog* 11:e1005204.
53. Phipps KL, Ganti K, Jacobs NT, Lee C-Y, Carnaccini S, White MC, Manandhar M, Pickett BE, Tan GS, Ferreri LM, Perez DR, Lowen AC. 2020. Collective interactions augment influenza A virus replication in a host-dependent manner. *bioRxiv*.

54. Phipps KL, Ganti K, Jacobs NT, Lee CY, Carnaccini S, White MC, Manandhar M, Pickett BE, Tan GS, Ferreri LM, Perez DR, Lowen AC. 2020. Collective interactions augment influenza A virus replication in a host-dependent manner. *Nat Microbiol* 5:1158-1169.
55. Fields BN. 1971. Temperature-sensitive mutants of reovirus type 3 features of genetic recombination. *Virology* 46:142-8.
56. Fields BN, Joklik WK. 1969. Isolation and preliminary genetic and biochemical characterization of temperature-sensitive mutants of reovirus. *Virology* 37:335-42.
57. Spandidos DA, Graham AF. 1976. Recombination between temperature-sensitive and deletion mutants of reovirus. *J Virol* 18:117-23.
58. Wenske EA, Chanock SJ, Krata L, Fields BN. 1985. Genetic reassortment of mammalian reoviruses in mice. *J Virol* 56:613-6.
59. Chao L, Tran TT, Tran TT. 1997. The advantage of sex in the RNA virus phi6. *Genetics* 147:953-9.
60. Chao L, Tran T, Matthews C. 1992. Muller's Ratchet and the Advantage of Sex in the Rna Virus 6. *Evolution* 46:289-299.
61. Chao L. 1990. Fitness of RNA virus decreased by Muller's ratchet. *Nature* 348:454-5.
62. Smith GJ, Vijaykrishna D, Bahl J, Lycett SJ, Worobey M, Pybus OG, Ma SK, Cheung CL, Raghvani J, Bhatt S, Peiris JS, Guan Y, Rambaut A. 2009. Origins and evolutionary genomics of the 2009 swine-origin H1N1 influenza A epidemic. *Nature* 459:1122-5.
63. Garten RJ, Davis CT, Russell CA, Shu B, Lindstrom S, Balish A, Sessions WM, Xu X, Skepner E, Deyde V, Okomo-Adhiambo M, Gubareva L, Barnes J, Smith CB, Emery SL, Hillman MJ, Rivaller P, Smagala J, de Graaf M, Burke DF, Fouchier RA, Pappas C, Alpuche-Aranda CM, Lopez-Gatell H, Olivera H, Lopez I, Myers CA, Faix D, Blair PJ, Yu C, Keene KM, Dotson PD, Jr., Boxrud D, Sambol AR, Abid SH, St George K, Bannerman T, Moore AL, Stringer DJ, Blevins P, Demmler-Harrison GJ, Ginsberg M, Kriner P, Waterman S, Smole S, Guevara HF, Belongia EA, Clark PA, Beatrice ST, Donis R, et al. 2009. Antigenic and genetic characteristics of swine-origin 2009 A(H1N1) influenza viruses circulating in humans. *Science* 325:197-201.
64. Ince WL, Gueye-Mbaye A, Bennink JR, Yewdell JW. 2013. Reassortment complements spontaneous mutation in influenza A virus NP and M1 genes to accelerate adaptation to a new host. *J Virol* 87:4330-8.
65. Harima H, Sasaki M, Kajihara M, Gonzalez G, Simulundu E, Bwalya EC, Qiu Y, Okuya K, Isono M, Orba Y, Takada A, Hang'ombe BM, Mweene AS, Sawa H. 2020. Characterization of mammalian orthoreoviruses isolated from faeces of pigs in Zambia. *J Gen Virol* 101:1027-1036.
66. Lelli D, Moreno A, Steyer A, Nagli c T, Chiapponi C, Prospero A, Faccin F, Sozzi E, Lavazza A. 2015. Detection and Characterization of a Novel Reassortant Mammalian Orthoreovirus in Bats in Europe. *Viruses* 7:5844-54.

67. Cross RK, Fields BN. 1976. Use of an aberrant polypeptide as a marker in three-factor crosses: further evidence for independent reassortment as the mechanism of recombination between temperature-sensitive mutants of reovirus type 3. *Virology* 74:345-62.
68. Boehme KW, Ikizler M, Kobayashi T, Dermody TS. 2011. Reverse genetics for mammalian reovirus. *Methods* 55:109-13.
69. Hockman MR, Phipps KL, Holmes KE, Lowen AC. 2020. A method for the unbiased quantification of reassortment in segmented viruses. *J Virol Methods* 280:113878.
70. Marshall N, Priyamvada L, Ende Z, Steel J, Lowen AC. 2013. Influenza virus reassortment occurs with high frequency in the absence of segment mismatch. *PLoS Pathog* 9:e1003421.

**Chapter II. A method for the unbiased quantification of reassortment in segmented viruses**

**Megan R. Hockman<sup>a</sup>, Kara L. Phipps<sup>a</sup>, Katie E. Holmes<sup>a</sup> and Anice C. Lowen<sup>a,b\*</sup>**

<sup>a</sup>Department of Microbiology and Immunology, Emory University School of Medicine, Atlanta, Georgia, United States of America

<sup>b</sup>Emory-UGA Center of Excellence for Influenza Research and Surveillance (CEIRS)

\*Corresponding Author: 1510 Clifton Rd, Atlanta, GA 30322; anice.lowen@emory.edu

The work of this chapter was published in the Journal of Virological Methods in 2020.

**Citation:**

MR, Phipps KL, Holmes KE, Lowen AC. A method for the unbiased quantification of reassortment in segmented viruses. *J Virol Methods*. 2020;280:113878. Epub 2020/05/01. doi: 10.1016/j.jviromet.2020.113878. PubMed PMID: 32353455; PubMed Central PMCID: PMC7296281.

## **Abstract**

Reassortment of segmented viruses can be an important source of genetic diversity underlying viral evolution and emergence. Methods for the quantification of reassortment have been described but are often cumbersome and best suited for the analysis of reassortment between highly divergent parental strains. While it is useful to understand the potential of divergent parents to reassort, outcomes of such heterologous reassortment are driven by differential selection acting on the progeny and are typically strain specific. To quantify reassortment robustly, a system free of differential selection is needed. We have generated such a system for influenza A virus and for mammalian orthoreovirus by constructing well-matched parental viruses carrying small genetic tags. The method utilizes high-resolution melt technology for the identification of reassortant viruses. Ease of sample preparation and data analysis enables streamlined genotyping of a large number of virus clones. The method described here thereby allows quantification of the efficiency of reassortment and can be applied to diverse segmented viruses.

## **Introduction**

Virus genome organization varies widely across different families. Segmented genomes, which are comprised of distinct RNA molecules, have been documented in eleven virus families to date. Segment numbers vary, as do replication strategies. Each genome segment encodes a different protein or proteins which are involved in establishing a productive infection. During infection, cells can be co-infected by multiple parent viruses. In segmented viruses, co-infection events have the potential to give rise to many different progeny genotypes, fueling evolution.

Viruses with segmented genomes undergo a type of genetic recombination termed reassortment. Reassortment occurs when two or more parent viruses co-infecting a single cell exchange whole gene segments, which are then packaged together to yield progeny viruses with novel genotypes.

This mode of generating diversity is unique to segmented viruses and contrasts with classical recombination, in which a chimeric genome is formed intramolecularly, through the combination of nucleic acid sequences derived from two viral genomes. Reassortment events most often yield attenuated progeny due to incompatibilities between nucleic acids and/or proteins derived from heterologous parents(1-5). There is, however, the potential for the coupling of compatible, beneficial alleles and the subsequent emergence of novel pathogens, as was observed in the 2009 influenza A virus (IAV) pandemic(6, 7).

To date, reassortment has been investigated in several viruses, including IAV and mammalian orthoreovirus (reovirus), using a variety of methods. Measurement of reassortment is often complicated by fitness differences among progeny viruses or a lack of sensitive quantification methods. In the former case, difficulties arise due to selection. When reassortment yields progeny of variable fitness, those with the most beneficial segment combinations will be amplified more rapidly. Preferential propagation of parental genotypes results in underestimation of the frequency of reassortment. Similarly, preferential amplification of certain reassortant viruses results in underestimation of population diversity. To avoid these issues, it is preferable to quantify reassortment between viruses of more similar genotypes. This can be challenging, however, as most detection methods rely on parental viruses being significantly different genetically. Detection of reassortment in genetically similar viruses requires sensitive molecular technologies, which were not available until relatively recently(8).

The earliest method to identify reassortants utilized polyacrylamide gel electrophoresis(9-11). This method depends on all segments of each parental genome having different electrophoretic mobility. Thus, each segment must differ significantly in length and/or sequence. This requirement for significant differences for detection necessitates that parent viruses are divergent, which – as discussed above – can impact the fitness of reassortant progeny and

reduce observed rates of reassortment. Additionally, there is a practical limitation on the number of samples that can feasibly be analyzed using this approach.

As an alternative approach, temperature-sensitive (ts) mutants have been used to quantify reassortment(12, 13). In this system, a single segment confers temperature-sensitivity in each parental virus and pairs of viruses used for co-infection carry ts mutations in differing segments. Temperature sensitivity is abrogated if these segments are exchanged for wild type segments from the opposite parent in a reassortment event. Culture of progeny viruses at the nonpermissive temperature results in selection of reassortants. Titration at the nonpermissive temperature therefore allows quantification of the frequency of exchange of the ts segments. This approach makes it possible to detect reassortment between identical parents (with the exception of the ts lesions), thus avoiding the confounding effects of protein or segment incompatibilities. However, it does not yield the frequency of reassortment between all virus segments but rather only the two ts segments(12, 14).

PCR-based methods can also be used to differentiate parental segments that differ sufficiently to allow the design of specific primers(15-17). Amplicons can be detected using gel electrophoresis with ethidium bromide staining or by determining  $C_t$  values in quantitative PCR. These methods may be limited when parental genomes are too similar to allow unique primer design for all segments.

Alternatively, whole or partial genome sequencing of clonal virus populations offers a very flexible approach to identify reassortants(18). With sequencing as a read-out, the need for primer design does not constrain the parental viruses that can be examined in combination. Traditionally, the costs of sequencing approaches have prohibited their use on a larger scale. In recent years, however, the price of sequencing has decreased and the technology has improved.

To address the shortcomings of prior methodologies and enable robust quantification of reassortment, we present here two methodological innovations. First, to eliminate selection bias, we generated well- matched pairs of parental viruses that differ only by one or a handful of synonymous mutations in each genome segment. These introduced synonymous changes act as genetic markers to indicate the parental origin of each segment. Second, to streamline the detection of reassortant viruses, we applied high resolution melt analysis, a post-PCR method originally developed to differentiate single nucleotide polymorphisms in eukaryotic genomes(8). Because this method is sensitive enough to detect single nucleotide differences, it allows for the quantification of reassortment between highly similar parental viruses. We have applied these approaches to both IAV and reovirus.

## **Results**

### ***Marker mutations in variant viruses do not cause fitness defects***

To quantify reassortment in the absence of selection bias, it is important to ensure that the parental viruses do not differ in fitness. If one virus is fitter, that parental genotype and segments from it are likely to predominate in the progeny virus population due to uneven amplification. This outcome may be of interest in some contexts but obscures quantitative analysis of reassortment itself. For IAV, single-cycle growth of wild-type and variant viruses was assessed in A549 cells. The two viruses showed similar growth properties, and a two-way ANOVA yielded a nonsignificant P-value of 0.94 when comparing the two curves (Figure 3). For reovirus, single-cycle growth in L929 cells was evaluated to compare variant and wild type viruses. Again in this system, the variant strain was not attenuated relative to the wild-type counterpart, with a two-way ANOVA yielding a P-value of 0.95 (Figure 3). Additionally, there was no noted difference in plaque phenotype for either virus (data not shown). The highly homologous genotypes and comparable fitness of parental viruses are expected to result in

similar fitness of reassortant progeny, allowing for an unbiased assessment of reassortment frequency.

***Flow cytometry allows quantification of the proportion of cells infected***

Owing to the presence of non-plaque forming particles in virus populations and routine experimental error, calculation of MOI based on plaque forming units does not always allow an accurate estimation of the proportion of a cell population that is infected. Flow cytometry analysis targeting viral antigens allows a more direct method to monitor infection levels.

In the case of IAV, the addition of different epitope tags to wt and var HA proteins allowed quantification of single- and co-infected cells within the population. Four distinct populations were observed representing uninfected, wild-type virus infected (expressing 6x HIS tag), variant virus infected (expressing HA tag), or wild type plus variant co-infected cells (Figure 4).

Assessment of the proportion of cells in a population that are co-infected is useful, as co-infected cells are the only ones capable of producing reassortant progeny.

Since insertion of epitope tags was not feasible in the reovirus system, flow cytometry of reovirus-infected cells was used to evaluate the proportion of cells that were infected, but no direct measurement of co-infected cells was made. Infected cells were detected using a primary antibody (clone 10C1) against viral structural protein  $\sigma_3$  and compared to an uninfected, stained control. Infected cells cluster within two groups with low and high antigen expression, respectively (Figure 4). To estimate the percentage of infected cells that are co-infected, Poisson statistics can be used, assuming an equal proportion of wild-type and variant viruses were present in the initial infection. We used the following to determine the expected fraction of infected cells that is co-infected with  $\lambda = -\ln(1 - \% \text{ infected cells})$ :

$$\sum_{v=1}^{\infty} \frac{e^{-\lambda} \lambda^v}{v!} (1 - 2 * 0.5^v)$$

An example of expected % co-infection based on % infected cells is given in Table 3.

### ***High-resolution melt analysis allows determination of viral genotypes***

High-resolution melt analysis allows detection of the nucleotide changes that differentiate wt and var viruses and can therefore be used for rapid assignment of wt or var genotypes to all segments present in clonal virus isolates. To this end, qPCR was performed with the cDNA of each viral isolate split into eight (IAV) or ten (reovirus) separate duplicate reactions, each containing primers targeting a different segment. Following qPCR, samples with  $C_t$  values below 35 were used for melt analysis. The included wt and var controls were used as references and clusters based on similarity of  $T_m$  and melt curve shape were generated within BioRad High Precision Melt software (Figure 5). The distinct melt curves of wt and var amplicons indicate that the silent mutations introduced were sufficient for identification of the parental origins of each segment (Figure 5). In practice, we find that a minimum  $T_m$  difference of  $0.15^\circ\text{C}$  is needed to consistently differentiate between wt and var amplicons. Applying this approach to each segment in turn allows the full genotype of each clonal plaque pick to be determined.

Full genotypes are depicted in reassortment tables where each column is a separate genome segment, and rows represent clonal isolates (Figure 6). Occasionally, high resolution melt analysis yielded unclear results, with a given amplicon clustering neither with wt nor var controls. While exact causes of indeterminate results are not clear, possibilities include isolation of RNA from a mixed plaque pick (which would result in a  $T_m$  intermediate between that of the wt and var amplicons), co-packaging of a segment from both parental viruses (although we consider this to be unlikely), low cDNA quantities or loading error during plate preparation.

Such results were recorded as indeterminate (white boxes in Figure 6). Viral isolates were excluded from analysis if there were more than two segments omitted due to unclear melt curves. If more than 20% of replicates were omitted from analysis, data collection was repeated starting from plaque picks.

Following assembly of genotype tables, the percent reassortment observed in each sample is calculated as 100 times the number of reassortant clones identified divided by the total number of clones genotyped. To visualize the relationship between infection and reassortment, the calculated percent reassortment can be plotted as a function of the percent infected cells as calculated by flow cytometry (Figure 7). Additionally, due to the introduction of differing epitope tags in wt and var viruses, IAV reassortment can be plotted as a function of the percent co-infected cells. This is a useful measure, as only co-infected cells are capable of yielding reassortant progeny. For this quantitative assessment of reassortment to be meaningful, it is important that co-infections be performed under single cycle conditions. As noted in the Materials and Methods section, this was achieved for IAV using addition of ammonium chloride to cell culture medium at 3 h post-infection and for reovirus using E64D protease inhibitor added at 4 h post-infection. Blocking secondary spread of progeny virus ensures that detected frequencies of reassortant viruses reflect the efficiency of reassortment, rather than the efficiency of amplification. In contexts where infection cannot be limited to a single cycle, such as in vivo, analysis of genotypic diversity (as described below) is more appropriate than a simple readout of percent reassortment.

### ***Diversity analysis quantifies richness and evenness of reassortant population***

A sample in which a single reassortant genotype is detected repeatedly would have high percent reassortment despite having low genotypic diversity. When using a wt/var co-infection system, this situation is unlikely to arise due to selection but can nevertheless occur under conditions

where stochastic effects are strong (e.g. owing to within-host bottlenecks *in vivo*). Here, the percent reassortment readout is not highly relevant and a more sophisticated analysis of genotypic diversity is needed.

To quantify the diversity of genotypes present, Simpson's index (given by  $D = \sum(p_i^2)$ , where  $p_i$  is the proportional abundance of each genotype) was used. This approach accounts for both the raw number of species (richness) and variation in the abundance of each (evenness) and is sensitive to the abundance of dominant species. To determine effective diversity, the Simpson index value of each sample was converted to a corresponding Hill number,  $N_2 = 1/D$ . The Hill number  $N_2$  is equivalent to the number of equally abundant species needed to generate the observed diversity in a sample community and is particularly useful because it scales linearly (i.e., a virus population with  $N_2 = 10$  is twice as diverse as one with  $N_2 = 5$ ). Hill's  $N_2$  therefore allows a more intuitive comparison between populations and is suitable for statistical analysis by basic linear regression methods(19). Diversity can be determined for each replicate and plotted as a function of percent infection (Figure 7). While the % reassortment and diversity plots shown here are similar, in cases where selection or drift have shaped the viral population, very different trends may be seen.

## **Discussion**

Here we outline a conceptually simple approach to accurately quantify reassortment between co-infecting segmented viruses in the absence of selection bias. Our strategy utilizes reverse genetics derived parental viruses designed to allow both unbiased reassortment and streamlined genotyping. This approach overcomes limitations of previous methods in which quantitative analysis of reassortment was impeded by fitness differences among progeny viruses. The genotyping technology employed furthermore improves upon more cumbersome procedures involving gel electrophoresis or temperature-sensitive mutants. This method is useful for fundamental studies of reassortment and other interactions within virus populations.

We have used this method to evaluate reassortment of Pan/99 IAV and T3D reovirus. At high MOI, both viruses showed abundant reassortment. Further studies are needed with reovirus to assess the impact of MOI on reassortment levels and thereby gain more quantitative insight into the efficiency of segment exchange in this system. For IAV, the data included herein allow analysis of the frequency of reassortment in A549 cells as a function of both infected and co-infected cells. In line with our previous observations in other cell types(20), IAV reassortment was high even at co-infection levels below 25%. High reassortment at low % co-infection goes against the expectation of models that assume an equivalent burst size for all infected cells(20). The results suggest that co-infected cells produce more progeny than singly infected cells, as a consequence of beneficial virus-virus interactions within the cell. We previously showed that complementation of incomplete viral genomes is one such interaction(21, 22). Whether a similar effect occurs for reovirus has yet to be determined.

In addition to its use for differentiating wt and var viruses herein, high resolution melt analysis can also be applied to viral genotyping in systems where highly divergent parental viruses undergo reassortment. Although fitness differences among progeny viruses will obscure the quantitative assessment of reassortment in such an experiment, monitoring the combined outcomes of reassortment and selection is often highly relevant for assessing the public health risks posed by reassortment of parental strains of interest(23-26). Highly divergent parental sequences are likely to exhibit detectable differences in melting properties, conducive to HRM analysis. It is important to note, however, that reciprocal changes within the region targeted for amplification and melt analysis will nullify differences in melting properties and therefore prohibit detection. Short regions with fewer single nucleotide polymorphisms are less likely to contain reciprocal changes and should be selected for amplification. In addition, regions of high homology must border the target region, as the same HRM primer set must be used for each parental virus. In practice for IAV, when considering reassortment between strains of differing subtypes, we found that HRM can be successfully applied to genotype the six non-HA, non-NA

segments. The low sequence identity across HA and NA subtypes precluded common primer design and an alternative genotyping approach was used for these segments(23).

Whole genome sequencing of clonal viral isolates is an alternative to the HRM approach that has been used recently to identify reassortant viruses(27). Next generation sequencing (NGS) allows parallel sequencing of all viral gene segments, which greatly reduces effort compared to classical Sanger sequencing. In addition, because viral genomes are typically small, the costs of NGS can be reduced by combining the barcoded cDNA derived from many isolates into a single sequencing lane. NGS can be applied to any pairing of parental viruses and may be more feasible than HRM where parental viruses are highly divergent and identical HRM primers cannot be generated for all segments. However, in experiments using matched parental viruses, such as the wt/var system, the HRM approach simplifies data collection. Whole genome sequencing requires additional preparation steps including the pre-amplification of cDNA, fragmentation and library generation. Additionally, customized bioinformatics approaches are necessary for NGS data analysis but not required in the HRM approach.

Segmented viruses utilize a variety of replication strategies which may impact their potential to undergo reassortment. For this reason, quantification of reassortment not only informs studies of viral diversification and evolution but can also offer insight into fundamental aspects of the virus life cycle. Reovirus, for example, replicates within cytoplasmic inclusions. These inclusions may prohibit exchange of gene segments and thus limit reassortment. High reassortment levels in this system would indicate an unknown role of inclusion dynamics or viral RNA trafficking in the life cycle. Other segmented viruses which are not known to form structured cytoplasmic inclusions may nevertheless possess organizational mechanisms which impact reassortment frequency. Deviation from the expectation that reassortment occurs freely at levels corresponding to the number of co-infected cells could indicate additional features of the virus' replication cycle that are important, such as the prevalence of incomplete viral genomes in

IAV(20-22, 28, 29). The role of compartmentalization and incomplete genomes in other virus families, such as the *Reoviridae*, remains incompletely understood, as does the frequency of reassortment in these systems. Utilization of the strategy outlined herein for monitoring reassortment may open up further avenues of study with respect to segmented virus replication mechanisms and population dynamics.

## **Materials and Methods**

### *Cell lines and cell culture media*

293T cells from the American Type Culture Collective (ATCC) were maintained in Dulbecco's Modified Eagle Medium (DMEM; Gibco) supplemented with 10% fetal bovine serum (FBS; Atlanta Biologicals). A549 cells (ATCC CCL-185) were maintained in F-12K nutrient mixture with L-glutamine (Corning) supplemented with 10% FBS and penicillin (100 IU), and streptomycin (100 ug/mL) (PS; Corning). Baby hamster kidney cells stably expressing T7 RNA polymerase (BHK-T7) cells(30) were maintained in DMEM supplemented with 5% FBS, 2 mM L-Glutamine (Corning), PS and 1 mg/mL G418 (Gibco). Spinner-adapted L929 cells (gift from Bernardo Mainou) were grown in Joklik's modified MEM supplemented with 5% FBS, 2 mM L-Glutamine, PS and 0.25 mg/mL amphotericin B (Sigma), termed SMEM.

### *Design of wild-type and variant viruses*

To allow quantitative analysis of reassortment, we designed parental viruses that are i) highly homologous, so that reassortment does not give rise to genetic or protein incompatibilities, and ii) genetically distinct in all segments to allow tracking of genetic exchange. For both IAV and reovirus, a variant virus was generated from the wild-type strain using reverse genetics. The wild type (wt) virus strains used were influenza A/Panama/2007/99 (H3N2) (Pan/99) virus and Type 3 Dearing (T3D) reovirus. To generate variant (var) viruses, silent mutations were added to the first 1kb of each wild-type virus coding sequence, as shown in Table 1. We have made multiple versions of the Pan/99var virus(31, 32); the Pan/99var virus described here is

Pan/99var15. The mutations made were A to G/G to A or C to T/T to C, which have the greatest impact on melting properties(8). The melting properties of a short amplicon (65-110 base pairs) containing a mutation of this nature is typically altered sufficiently to allow robust detection by high resolution melt analysis(8, 23). The change in melting properties of the short amplicon is dependent upon the amplicon sequence and the nature of the nucleotide change, with multiple changes in the same direction (ex. A → G and T → C) typically resulting in a greater  $T_m$  difference. To avoid introducing attenuating mutations, sites of natural variation were targeted where sequence data was available. For IAV, isolates from the same lineage within a 10-year time frame were selected from the NCBI GenBank database, and 20-30 sequences were aligned. Sites within the first 1000 nucleotides relative to the 3' end of the vRNA that displayed high nucleotide diversity were targeted for introduction of variant mutations. Point mutations were introduced into plasmid-encoded viral cDNAs using QuikChange mutagenesis (Agilent) according to the manufacturer's protocol.

To distinguish infected cells by flow cytometry, sequences encoding a 6xHIS or an HA epitope tag were added to the N-terminus of the IAV hemagglutinin protein, connected by a GGGGS linker sequence(33). The 6xHIS tag was added to the Pan/99wt virus and the HA tag was added to the Pan/99var15 virus. The linker sequence provides flexibility so that the epitope tags do not interfere with HA protein folding. To ensure the tags were retained on the mature HA proteins, they were inserted after the signal sequence. It was not possible to add an epitope tag to reovirus, as this has been demonstrated in the literature and in our hands to cause growth defects (data not shown)(34).

#### *Generation of virus stocks*

IAVs were generated by reverse genetics from viral cDNA(35, 36). Eight pPOL1 reverse genetics plasmids encoding the eight viral cDNAs were combined with four pCAGGS protein expression vectors encoding PB2, PB1, PA, and NP proteins. These plasmids were co-transfected into 293T

cells using XtremeGene transfection reagent (Sigma-Aldrich) according to the manufacturer's recommended procedure. At 16-24 h post transfection, the 293T cells were resuspended in growth medium and injected into the allantoic cavity of 9-11 day old embryonated chicken eggs (Hy-Line). Eggs were incubated 40 h in a humidified 33°C incubator. Incubation at 33°C was used because we have observed improved growth of the Pan/99 strain at this temperature, compared to 37°C (37). After chilling eggs overnight at 4°C, allantoic fluid was harvested, clarified of cell debris and aliquoted for storage at -80°C.

Reoviruses were generated from viral cDNA cloned into the pT7 plasmid in BHK-T7 cells(38). Plasmids containing each of the 10 viral cDNA's and pCAG FAST P10 plasmid were transfected into BHK-T7 cells using TransIT-LT1 (Mirus)(39). Cells were fed with an additional 500 µL SMEM on day 2. BHK-T7 cells were incubated at 37°C for a total of 5 days, after which virus was harvested with 3 freeze-thaw cycles at -80°C. Plaque assays were performed using viral lysates as previously described(40). Reoviruses were amplified for two passages in L929 cells(40). Purified virus stocks were made from second passage L929 lysates. Purification was performed as described previously using Vertrel XF extraction and a CsCl density gradient(41). The band at 1.36 g/cm<sup>3</sup> was collected and dialyzed exhaustively against virus storage buffer (15mM NaCl, 15mM MgCl<sub>2</sub>, 10mM Tris-HCl [pH 7.4]). The resultant purified material was stored in glass vials at 4°C for up to six months.

#### *Analysis of single-cycle growth*

To synchronize the infections, inoculation and virus attachment were performed on ice prior to warming dishes for viral entry. To limit viral growth to a single cycle, NH<sub>4</sub>Cl was added to the medium for IAV experiments and either NH<sub>4</sub>Cl or the protease inhibitor E64D was added for reovirus experiments. The details of these treatments are given below.

IAV

A549 cells were seeded at a density of  $4 \times 10^5$  cells per well in 6-well dishes 24 h prior to infection, with three wells prepared per virus. Stocks of Pan/99var15 and Pan/99wt viruses were individually diluted to achieve an MOI of 5 PFU/cell in 200  $\mu$ L 1X PBS per well. Growth medium was aspirated from the cells, and cells were washed three times with 1X PBS, with the third wash performed on ice. The dishes were kept on ice for inoculation and three wells per virus were inoculated with diluted virus. Cells were incubated at 4°C for 45 minutes to permit viral attachment, and dishes were rocked every 10 minutes during incubation. Cells were then placed back on ice, and inocula were removed before washing the cells three times with cold 1X PBS. Dishes were then removed from ice, and warm virus medium (2 mL) was added to each well, followed by incubation at 33°C for 2 h. Virus medium was removed, and acid inactivation to remove residual extracellular virus particles was performed by applying 0.5 mL PBS-HCl (pH 3.0) to each well. Cells were incubated at 33°C for 5 minutes, then PBS-HCl was removed. Virus medium (2 mL per well) was again added to each well. After incubation at 33°C for 1 h, virus medium was removed and replaced with 2 mL virus medium containing NH<sub>4</sub>Cl (20 mM) and HEPES buffer (50 mM) to ensure single cycle growth. Cells were incubated at 33°C for the duration of the growth curve, and a sample of cell supernatant (120  $\mu$ L) was taken from each well at 2, 6, 12, 16, 24, 36, and 48 h post-infection. Samples were stored at -80°C and thawed once prior to plaque assay in MDCK cells for titer determination.

#### Reovirus

L929 cells were seeded at a density of  $2.5 \times 10^5$  cells per well in 24 well dishes 24 h prior to infection. One plate was prepared for each time point, with 3 wells per plate dedicated to each virus. Inocula of T3Dwt and T3Dvar were prepared separately in OPTI-MEM, for an MOI of 10 PFU/cell in each well. Cells were placed on ice, washed once with 1X PBS, and 100  $\mu$ L of virus inoculum was added to each well. Virus was allowed to attach for 1 h at 4°C, and plates were rocked every 10 minutes during incubation. Cells were placed back on ice, inoculum was

removed, and cells were washed 3 times with cold 1X PBS. Next, 500  $\mu$ L of warm SMEM was added to each well, and cells were placed at 37°C. Starting at 0 h post infection, one plate was placed at -80°C every 3 h. At 4 h, SMEM was removed and replaced with SMEM containing 20 mM NH<sub>4</sub>Cl. Samples were freeze-thawed 3 times at -80°C, and titers at each time point were determined using a plaque assay in L929 cells.

### *Primers*

#### Reverse Transcription

For IAV, reverse transcription was performed using universal primers that anneal to the 3' end of all eight IAV vRNA's (GCGCGCAGC[A/G]AAAGCAGG) (42). Due to a lack of universally homologous sequences in reovirus, random hexamer primers (Thermo) were used in place of virus-specific primers.

#### High-resolution melt

Primers for quantitative PCR followed by high-resolution melt analysis were designed to flank the polymorphisms introduced into variant viruses. These primers were designed such that the amplicon size would be 65–110 base pairs and annealing temperatures were 58–62°C. Primer sequences for IAV and reovirus are listed in Table 2. Primer mixes were made by combining 5  $\mu$ L of the 100  $\mu$ M forward primer stock and 5  $\mu$ L of the 100  $\mu$ M reverse primer stock with 240  $\mu$ L molecular biology grade water for a final concentration of 4  $\mu$ M.

### *Co-infection*

#### IAV

Co-infections were performed with wild-type and variant (wt/var) viruses mixed at a 1:1 ratio and then diluted in PBS such that the total PFU/mL would give the desired multiplicity of infection. A549 cells seeded at a density of 4x10<sup>5</sup> cells/well in 6-well dishes 24 h prior to

infection were infected under single-cycle, synchronized conditions as detailed above for the growth analyses. These conditions include inoculation on ice (for synchronization), acid treatment (for inactivation of residual inoculum virus) and addition of  $\text{NH}_4\text{Cl}$ -containing medium at 3 h post infection (to prevent acidification of the endocytic compartment and thus multiple cycles of infection). At 12 h post infection, supernatants were collected and stored at  $-80^\circ\text{C}$ . Cells were harvested and prepared for analysis by flow cytometry.

### Reovirus

Co-infections followed the above procedure for synchronized, single-cycle infections. L929 cells were seeded in 12-well dishes at a density of  $1.8 \times 10^5$  cells/well 24 h prior to infection. The virus inoculum containing equal parts of wt/var virus as in IAV (above) was prepared in OPTI-MEM (Gibco), and cells were incubated in SMEM at  $37^\circ\text{C}$ . Rather than ammonium chloride, E64D protease inhibitor (Sigma) was added at a final concentration of  $4 \mu\text{M}$  at 4 h post infection to block secondary infection. At 24 h post infection, three replicate wells of reovirus-infected cells at each MOI were harvested for flow cytometry, and the remaining three replicates were freeze-thawed 3 times at  $-80^\circ\text{C}$  to release virus, and lysates stored at  $-80^\circ\text{C}$  for future analysis.

### *Flow cytometry to quantify infected cells*

#### IAV

Cells were harvested by the addition of  $200 \mu\text{L}$  trypsin (Corning) and, once cells were detached,  $800 \mu\text{L}$  FACS buffer (1X PBS with 2% FBS). Cells were transferred to 1.5 mL tubes on ice and pelleted by spinning at 1500 rpm for 3 minutes in a Beckman Coulter Microfuge 22R tabletop centrifuge. Supernatant was removed, and cells were washed two more times with 1 mL FACS buffer and  $200 \mu\text{L}$  FACS buffer, respectively, pelleting and removing supernatant between washes. After washes, cells were resuspended in  $50 \mu\text{L}$  stain buffer (FACS buffer containing Qiagen Penta-HIS Alexa Fluor 647 #35370 at a final concentration of  $5 \mu\text{g}/\text{mL}$  and Sigma-

Aldrich Monoclonal Anti-HA-FITC, Clone HA-7 #H7411 at a final concentration of 7  $\mu\text{g}/\text{mL}$ ) on ice in the dark for 35-45 minutes. Cells were washed twice with 200  $\mu\text{L}$  of FACS buffer and resuspended in FACS buffer for analysis.

### Reovirus

Cells were trypsinized and washed two times with FACS buffer, as above. Fixation, permeabilization, and staining were performed according to the BD Cytofix/Cytoperm protocol including a 15-minute block step with BD rat anti-mouse CD16/CD32 Fc block. To stain infected cells, a mouse monoclonal anti- $\sigma 3$  antibody (clone 10C1) at a concentration of 1  $\mu\text{g}/\text{mL}$  was added for 30 minutes at 4°C. After two washes, an AlexaFluor-647 conjugated donkey anti-mouse secondary antibody (Invitrogen) was added at a 1:1000 dilution.

In both virus systems, data was collected on a BD LSR II Flow cytometer running FACS Diva software. A minimum of 50,000 events was collected for each sample. Subsequent data analysis was performed using FlowJo (v10.1), gating for single cells. The threshold for positivity was determined based on a mock-infected control population stained with the relevant antibodies.

### *Viral genotyping*

#### Collection of clonal isolates

For both reovirus and IAV, samples stored at -80°C were thawed and plaque assays were performed as previously described(40). Individual, well-isolated plaques were picked by aspirating the agar plug using a 1 mL pipette and deposited into 160  $\mu\text{L}$  PBS in a 96-well assay block with 1 ml capacity wells (Costar 3958). From each sample, 21 plaques were picked for IAV, while 32 were picked for reovirus. Additionally, a single wild-type and a single variant plaque were included as controls for each series of 21 or 32 plaque picks. Assay blocks containing plaque isolates can be sealed and stored at -20°C or used directly for RNA extraction.

#### RNA extraction

RNA was extracted directly from agar plugs. Frozen assay blocks were thawed in a 37°C water bath and spun down at 2000 rpm for 2 min in a Heraeus Megafuge 16 tabletop centrifuge equipped with Thermo M-20 swinging bucket plate rotor. The Zymo *Quick*-RNA Viral Kit extraction protocol was followed using 96-well plates. Filter and collection plates were provided with the kit. No DNA/RNA Shield was used. Samples were eluted in 40 µL nuclease-free water into MicroAmp Optical 96-well reaction plates (Applied Biosystems). RNA can be covered and stored at -80°C or used directly for reverse transcription.

### Reverse Transcription

Working on ice, a 12.8 µL volume of each viral RNA sample was combined with Maxima RT buffer at a final concentration of 1X, dNTP's at a final concentration of 0.5 mM, either IAV primer at a final concentration of 0.3 µM or random hexamers (Thermo SO142) at a final concentration of 5 µM for reovirus, 100 U Maxima RT (Thermo), and 28 U RiboLock RNase inhibitor (Thermo). Total reaction volume was 20 µL. Samples were capped, mixed by vortexing, and spun down briefly. Reactions were incubated at 55°C for 30 minutes and 85°C for 10 minutes in a BioRad T100 thermocycler. cDNA can then be stored at -20°C or used directly for qPCR and high-resolution melt analysis.

### qPCR and high-resolution melt analysis

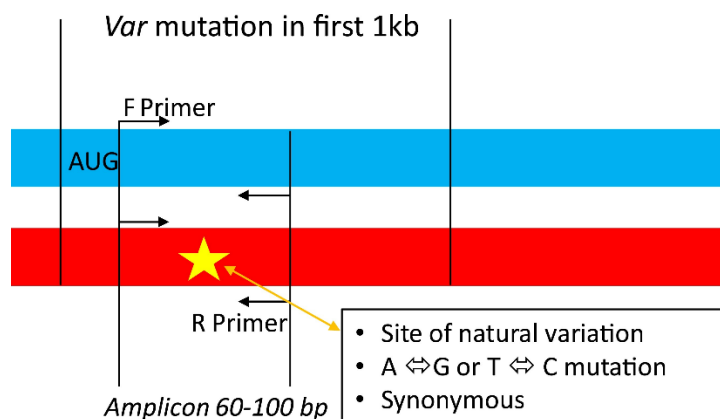
Viral cDNA was used as a template in qPCR reactions. Separate reactions were set up with primers targeting each of the viral gene segments. First, master mixes were made by combining appropriate primer mixes (see Table 2) with BioRad Precision Melt Supermix at volumes sufficient for the number of samples plus 15% extra. For each well, 0.5 µL of a 4 µM primer mixture containing both the forward and reverse primers was added to 2.5 µL Supermix. A 3 µL volume of this master mix was loaded into a 384 well plate (BioRad HSP3805) using a multichannel pipette according to the layouts in Figure 2. A 2 µL volume of cDNA diluted 1:4 (IAV) or 1:5 (reovirus) in molecular biology grade water (Invitrogen) was added to the 384 well

plate. Plates were centrifuged at 2600 rpm in a Heraeus Megafuge 16 tabletop centrifuge equipped with Thermo M-20 swinging bucket plate rotor for 3 minutes to collect liquid in the bottom of wells and remove bubbles. qPCR and melt analysis were performed using a BioRad CFX384 Real-Time PCR Detection System. Amplicons were generated by initial denaturation at 95°C for 2 min, then 40 cycles of 95°C for 10 s and 60°C for 30 s. Melting properties of PCR amplicons were examined by heating from 67°C to 90°C in 0.2°C increments. Successful amplification of targets was verified in CFX Manager software (BioRad). Melt curves were analyzed using Precision Melt Analysis software (BioRad) to determine viral genotypes.

### **Acknowledgements**

This work was funded in part by the NIH/NIAID Centers of Excellence for Influenza Research and Surveillance (CEIRS) contract HHSN272201400004C and NIH grant R01AI125268 to AL. We thank Bernardo Mainou and Nathan Jacobs for helpful discussion.

## Figures and tables



**Figure 1.** Design of variant mutations

Genome segments are indicated by blue (wt) and red (var) bars. The single nucleotide polymorphism is indicated by a star in the variant segment. Vertical lines indicate the 1 kb region (beginning at the start codon) in which the polymorphism was introduced, and the borders of the amplicon used in qPCR and subsequent high resolution melt analysis. Arrows indicate the directionality of the qPCR primers. Criteria used in the selection of the variant mutation position are indicated in the box on the lower right.

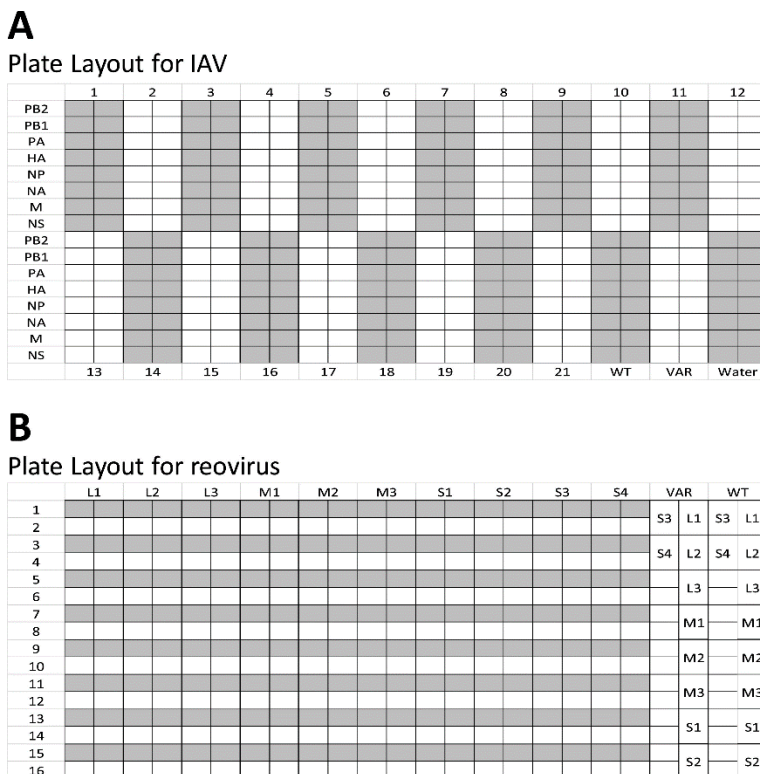


**Figure 2.** Example 384-well plate layouts for high-resolution melt analysis.

(A) Example plate layout for the analysis of IAV reassortment. Each plate holds 21 unknown samples (indicated by numbers at the top and bottom of each schematic plate), wt and var positive controls (bottom right) and a negative control in which water was loaded in place of cDNA (bottom right). Each of the 8 segments are analyzed in duplicate for each sample, in rows as indicated at the left with segment designations. (B) Example plate layout for the analysis of reovirus reassortment. Each plate holds 16 samples (indicated by numbers to the left), and wt and var positive controls (right side of the diagram). Each of the 10 segments are analyzed in duplicate, indicated by segment identification across the top and in wells for positive controls. Since 32 isolates are analyzed for reovirus reassortment, two plates must be used.

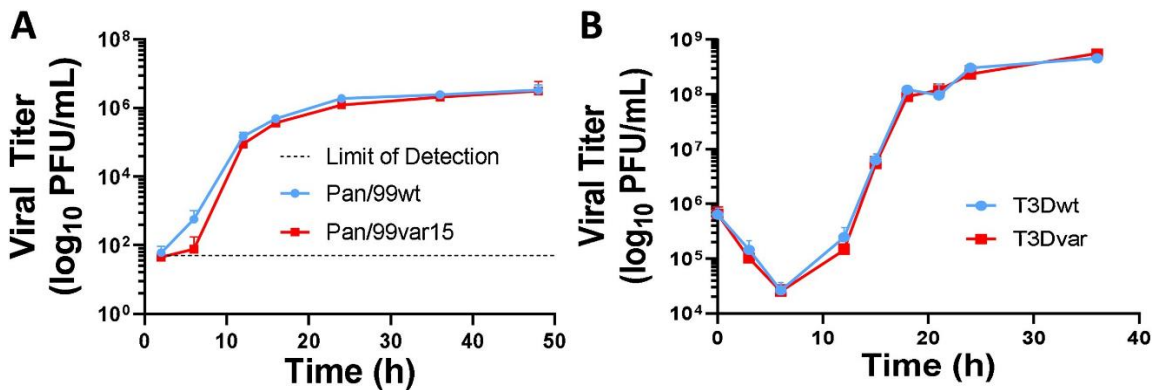


**Figure 3.** Single nucleotide changes do not detectably alter variant virus growth.

(A) Pan/99 IAV wild-type and variant multi-cycle growth were analyzed under single-cycle conditions in A549 cells over the course of 48 h (N = 3 for both viruses). (B) T3D mammalian orthoreovirus wild-type and variant virus growth were analyzed under single-cycle conditions in L929 cells over the course of 36 h (N = 3 for both viruses). Means are plotted and error bars represent standard deviation.

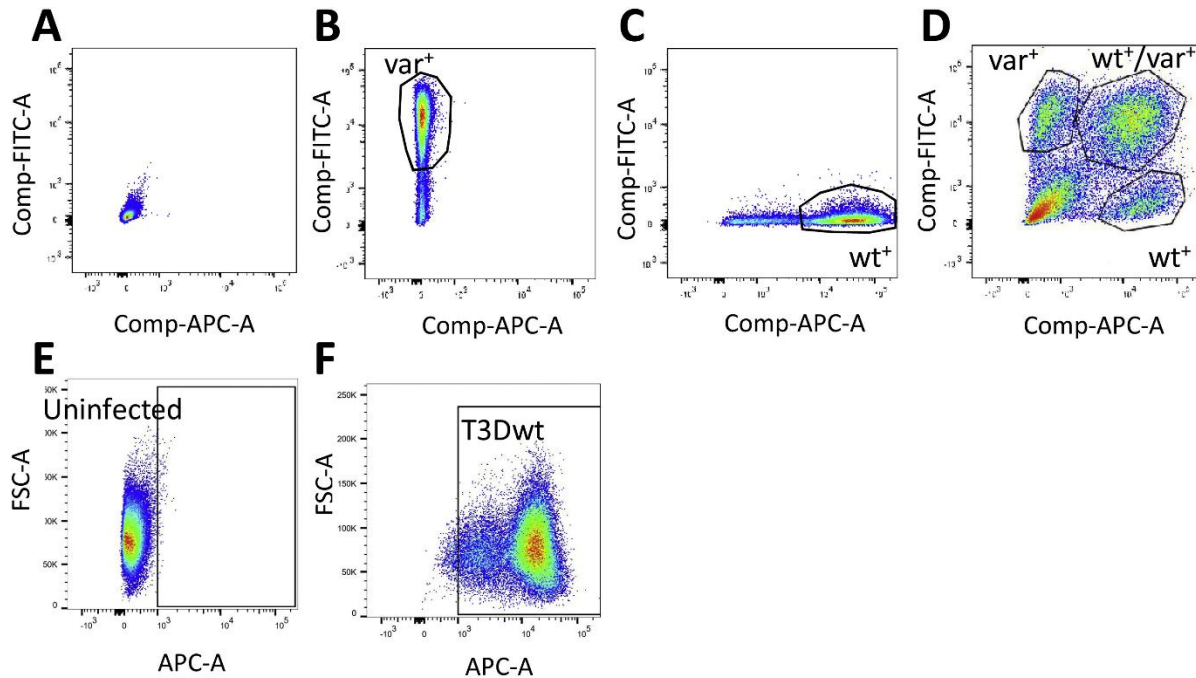


**Figure 4.** Flow cytometry allows for the quantification of infected and co-infected cells in a population.

(A) Uninfected cells, (B) Pan/99var15 infected cells, and (C) Pan/99 wt infected cells were used to determine the appropriate gate locations for (D) IAV co-infected cells. Populations of cells infected by a single virus are indicated by the top left- and bottom rightmost gates. Co-infected cells expressing both the HA and 6xHIS epitope tags are shown in the top rightmost gate. (E) Uninfected cells were used to determine the appropriate gate location for (F) reovirus infected cells. The population shift indicates 98.6 % infected cells divided between two populations, representing high and low levels of viral antigen expression.

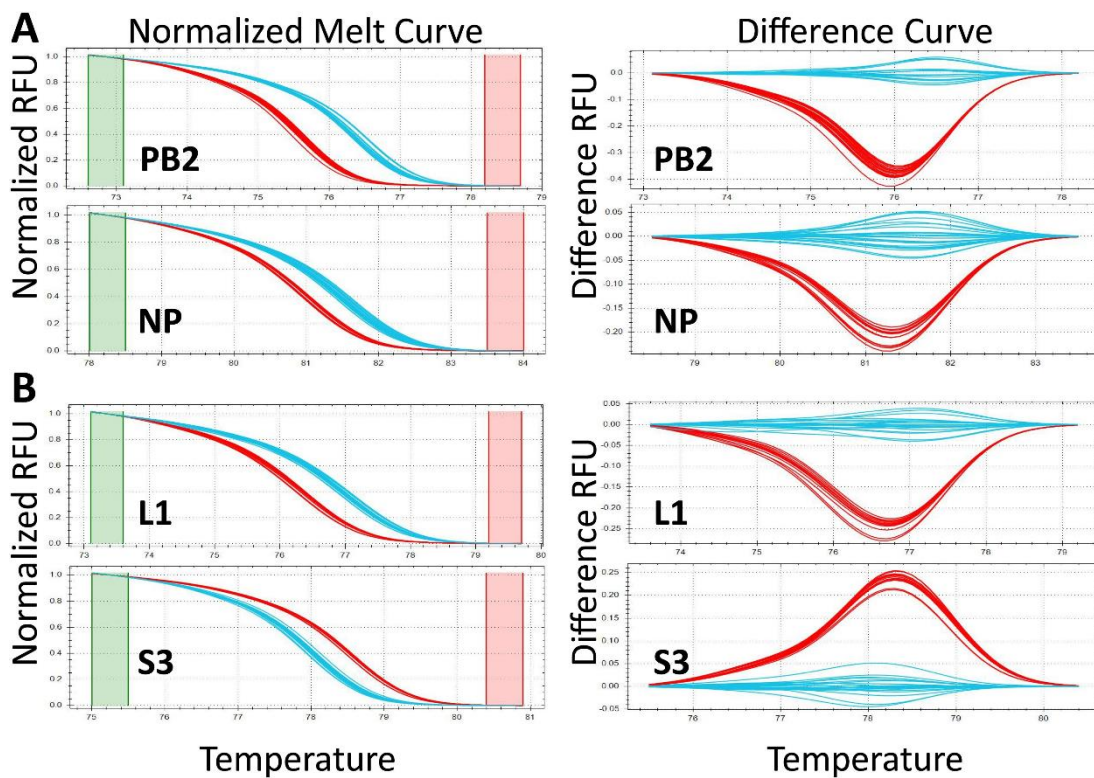


**Figure 5.** Melt curves allow the determination of parental segment origin.

Melt curves on the left indicating relative fluorescent units (RFU) as a function of temperature were used to generate the difference curves on the right, which enabled differentiation of wt and var segments in the clusters. Wild-type (blue) and variant (red) controls were used to determine the parental origins of each segment. Melt curves of the PB2 and NP segments from IAV (A) and the L1 and S3 segments from reovirus (B) are shown.

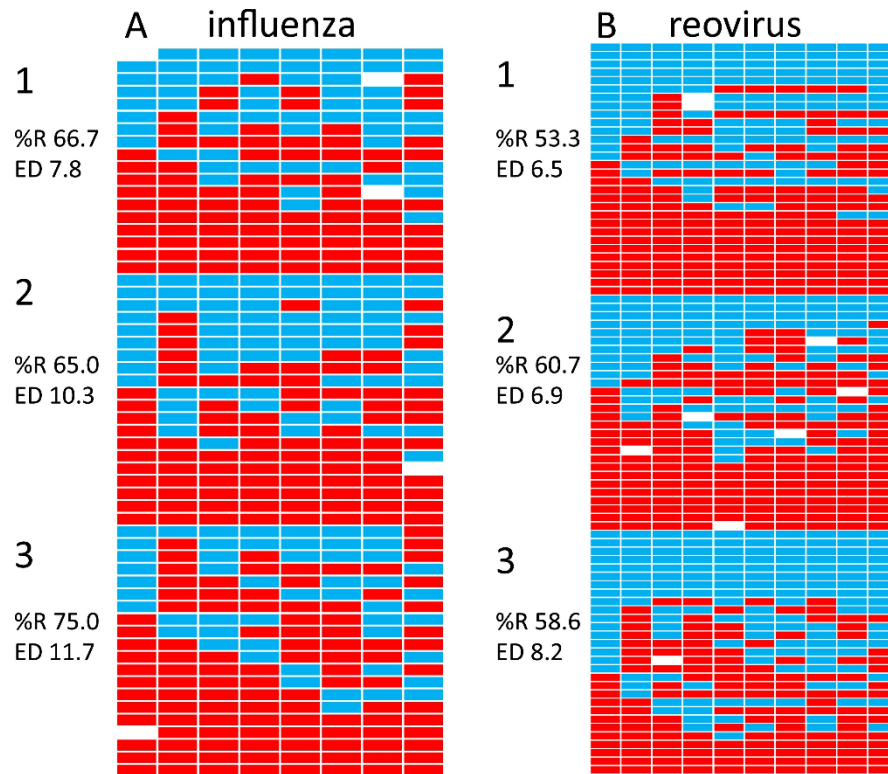


**Figure 6.** Reassortment tables provide visual representation of progeny virus genotypes. Each co-infection was performed in triplicate, and 21 (IAV) or 32 (reovirus) plaques were genotyped from each replicate. Blocks of genotypes numbered 1, 2 and 3 represent each replicate co-infection. Each row corresponds to a separate plaque isolate, and each column represents a gene segment (IAV segment order: PB2, PB1, PA, HA, NP, NA, M, NS; Reovirus segment order: L1, L2, L3, M1, M2, M3, S1, S2, S3, S4). Representative data from co-infections performed at a single MOI of both IAV (A) and reovirus (B) are shown. An MOI of 0.6 PFU/cell is shown for IAV, and an MOI of 3.16 PFU/cell is shown for reovirus. The calculated percent reassortment (%R) and the effective diversity (ED) as measured by Simpson's index are indicated for each replicate. Blue boxes indicate wild-type parental segment origin, red boxes indicate variant parental segment origin, and white boxes indicate indeterminate results.

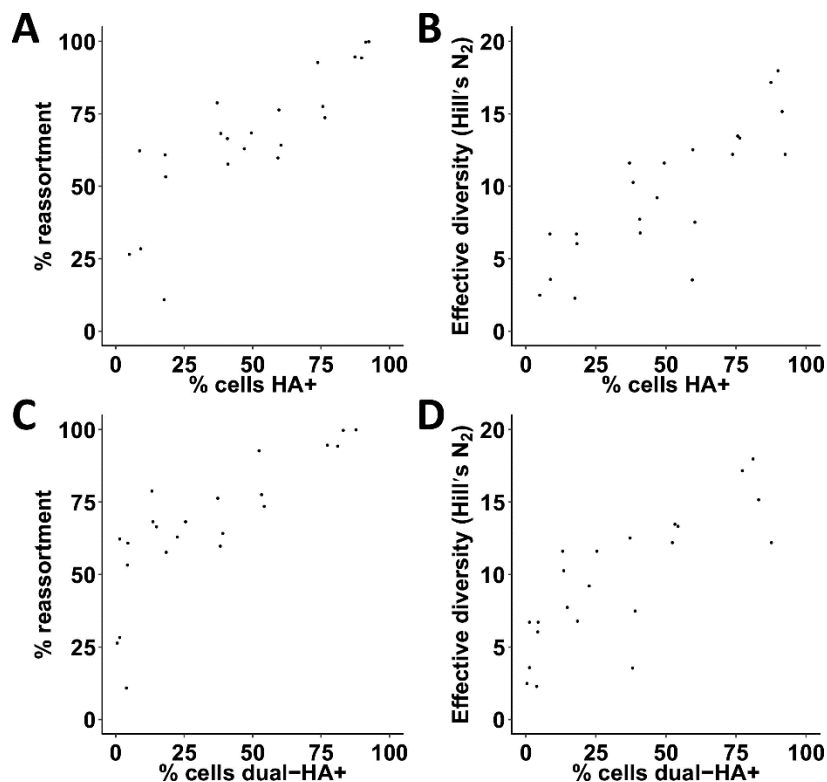


**Figure 7.** Comparison of IAV infection levels and reassortment.

Quantification of infected cells by flow cytometry can be combined with reassortment data to give insight into the dependence of reassortment on effective viral dose. (A) Percent reassortment as a function of the percentage of cells infected with Pan/99 wt and/or var viruses. (B) The effective diversity of Pan/99 isolates after co-infections in A549 cells as a function of the percentage of cells infected with Pan/99 wt and/or var viruses. (C) Percent reassortment as a function of the percentage of cells co-infected with Pan/99 wt and var viruses. (D) The effective diversity of Pan/99 isolates after co-infections in A549 cells as a function of the percentage of cells co-infected with Pan/99 wt and var viruses. Diversity increases more than five-fold from the lowest % infection to the highest in both (B) and (D).

**Table 1: Point mutations used to generate variant viruses**

<b>T3D Mammalian Orthoreovirus</b>		<b>Pan/99 Influenza A Virus</b>	
Segment	Polymorphism	Segment	Polymorphism(s)*
L1	C612T	PB2	C354T C360T
L2	C853T	PB1	A540G
L3	G481A	PA	A342G G333A
M1	C919T	HA	T308C C311A C314T A646T C467G T470A
M2	A650G	NP	C537T T538A C539G
M3	T702C	NA	C418G T421A A424C
S1	G312A	M	G586A
S2	A438G	NS	C329T C335T A341G
S3	T318C		
S4	C383T		

\* Note, although a single nucleotide tide change is sufficient to support HRM genotyping, the Pan/99var15 virus contains multiple changes in a number of segments owing to use of alternative genotyping approaches during development of the IAV system.

**Table 2: Primers used to generate amplicons for high-resolution melt analysis**

T3D Mammalian Orthoreovirus		
Segment	Forward Primer	Reverse Primer
L1	570F GCATAATTGCCCTTTATGGTG	624R AAGGTGCCCGATCTGGTAAT
L2	832F GCAACCCGTTACACGCTTAG	906R TAACACCCCAACCGATATG
L3	451F TCAGAAGCCGATGTCTACCA	539R TGATACCCATGACCACTGCT
M1	839F TTGATGCATTTGCCTTACCA	923R CATCGGCCACATCCACTAC
M2	606F AGAGTGGCTCAAACGTTGCT	659R TCACTACCGACTGCATTGGA
M3	643F GGGATAATGAAGGCTGCTGA	720R ACCGCCCCTCGTTATAGATT
S1	278F GAGCCCTCCAAACAGTTGTC	329R AAGTTGTCCCACTCGAGCAC
S2	415F CTAGCGCGTGATCCAAGATT	488R GTAGGAAATCGGGCCAAAAC
S3	266F GGGATATCCTTCAGACTCGTG	334R CTCATGGTGGATGCTTGATG
S4	323F GGGTATGCTGTCCTTCGTTG	391R ACCTCCCTCAGTACGCACAC
Pan99 IAV		
Segment	Forward Primer	Reverse Primer
PB2	322F TGGAATAGAAATGGACCTGTGA	414R GGTTCATGTTTTAACCTTTCG
PB1	508F AGGCTAATAGATTTCCCTCAAGGATG	596R ACTCTCCTTTTTCTTTGAAAGTGTG

---

PA	307F	398R
	TGCAACACTACTGGAGCTGAG	CTCCTTGTCACTCCAATTTTCG
HA	251F	313R
	CCTTGATGGAGAAAAGTGCAC	CAACAAAAGGTCCCATTCC
NP	482F	571R
	CAACATACCAGAGGACAAGAGC	ACCTTCTAGGGAGGGTCGAG
NA	386F	461R
	TCATGCGATCCTGACAAGTG	TGTCATTTGAATGCCTGTTG
M	563F	662R
	GTTTTGGCCAGCACTACAGC	CCATTTGCCTGGCCTGACTA
NS	252F	342R
	ACCTGCTTCGCGATACATAAC	AGGGGTCCTTCCACTTTTTG

---

**Table 3: Expected % co-infection from Poisson statistics**

<u>% infection<sup>1</sup></u>	<u>Expected % co-infection<sup>2</sup></u>
1	0.002
5	0.06
10	0.26
25	1.79
50	8.57
75	25
100	99.99

<sup>1</sup>The percent of infected cells as determined by flow cytometry analysis

<sup>2</sup>The predicted percentage of cells infected with both wt and var viruses

## References

1. McDonald SM, Aguayo D, Gonzalez-Nilo FD, Patton JT. 2009. Shared and group-specific features of the rotavirus RNA polymerase reveal potential determinants of gene reassortment restriction. *J Virol* 83:6135-48.
2. White MC, Lowen AC. 2018. Implications of segment mismatch for influenza A virus evolution. *J Gen Virol* 99:3-16.
3. Villa M, Lassig M. 2017. Fitness cost of reassortment in human influenza. *PLoS Pathog* 13:e1006685.
4. Lubeck MD, Palese P, Schulman JL. 1979. Nonrandom association of parental genes in influenza A virus recombinants. *Virology* 95:269-74.
5. Nibert ML, Margraf RL, Coombs KM. 1996. Nonrandom segregation of parental alleles in reovirus reassortants. *J Virol* 70:7295-300.
6. Smith GJ, Vijaykrishna D, Bahl J, Lycett SJ, Worobey M, Pybus OG, Ma SK, Cheung CL, Raghwani J, Bhatt S, Peiris JS, Guan Y, Rambaut A. 2009. Origins and evolutionary genomics of the 2009 swine-origin H1N1 influenza A epidemic. *Nature* 459:1122-5.
7. Garten RJ, Davis CT, Russell CA, Shu B, Lindstrom S, Balish A, Sessions WM, Xu X, Skepner E, Deyde V, Okomo-Adhiambo M, Gubareva L, Barnes J, Smith CB, Emery SL, Hillman MJ, Rivaller P, Smagala J, de Graaf M, Burke DF, Fouchier RA, Pappas C, Alpuche-Aranda CM, Lopez-Gatell H, Olivera H, Lopez I, Myers CA, Faix D, Blair PJ, Yu C, Keene KM, Dotson PD, Jr., Boxrud D, Sambol AR, Abid SH, St George K, Bannerman T, Moore AL, Stringer DJ, Blevins P, Demmler-Harrison GJ, Ginsberg M, Kriner P, Waterman S, Smole S, Guevara HF, Belongia EA, Clark PA, Beatrice ST, Donis R, et al. 2009. Antigenic and genetic characteristics of swine-origin 2009 A(H1N1) influenza viruses circulating in humans. *Science* 325:197-201.
8. Wittwer CT, Reed GH, Gundry CN, Vandersteen JG, Pryor RJ. 2003. High-resolution genotyping by amplicon melting analysis using LCGreen. *Clin Chem* 49:853-60.
9. Palese P, Schulman JL. 1976. Differences in RNA patterns of influenza A viruses. *J Virol* 17:876-84.
10. Ramig RF, Cross RK, Fields BN. 1977. Genome RNAs and polypeptides of reovirus serotypes 1, 2, and 3. *J Virol* 22:726-33.
11. Rodger SM, Holmes IH. 1979. Comparison of the Genomes of Simian, Bovine, and Human Rotaviruses by Gel-Electrophoresis and Detection of Genomic Variation among Bovine Isolates. *Journal of Virology* 30:839-846.
12. Fields BN. 1971. Temperature-sensitive mutants of reovirus type 3 features of genetic recombination. *Virology* 46:142-8.
13. Kendal AP, Cox NJ, Galphin JC, Maassab HF. 1979. Comparative studies of wild-type and cold-mutant (temperature-sensitive) influenza viruses: independent segregation of temperature-sensitivity of virus replication from temperature-sensitivity of virion

- transcriptase activity during recombination of mutant A/Ann Arbor/6/60 with wild-type H3N2 strains. *J Gen Virol* 44:443-56.
14. Fields BN, Joklik WK. 1969. Isolation and preliminary genetic and biochemical characterization of temperature-sensitive mutants of reovirus. *Virology* 37:335-42.
  15. Jackson S, Van Hoeven N, Chen LM, Maines TR, Cox NJ, Katz JM, Donis RO. 2009. Reassortment between avian H5N1 and human H3N2 influenza viruses in ferrets: a public health risk assessment. *J Virol* 83:8131-40.
  16. Dlugolenski D, Jones L, Tompkins SM, Crameri G, Wang LF, Tripp RA. 2013. Bat cells from *Pteropus alecto* are susceptible to influenza A virus infection and reassortment. *Influenza Other Respir Viruses* 7:900-3.
  17. Stincarelli M, Arvia R, De Marco MA, Clausi V, Corcioli F, Cotti C, Delogu M, Donatelli I, Azzi A, Giannecchini S. 2013. Reassortment ability of the 2009 pandemic H1N1 influenza virus with circulating human and avian influenza viruses: public health risk implications. *Virus Res* 175:151-4.
  18. Dung TTN, Duy PT, Sessions OM, Sangumathi UK, Phat VV, Tam PTT, To NTN, Phuc TM, Hong Chau TT, Chau NNM, Minh NN, Thwaites GE, Rabaa MA, Baker S. 2017. A universal genome sequencing method for rotavirus A from human fecal samples which identifies segment reassortment and multi-genotype mixed infection. *BMC Genomics* 18:324.
  19. Jost L. 2006. Entropy and diversity. *Oikos* 113:363-375.
  20. Fonville JM, Marshall N, Tao H, Steel J, Lowen AC. 2015. Influenza Virus Reassortment Is Enhanced by Semi-infectious Particles but Can Be Suppressed by Defective Interfering Particles. *PLoS Pathog* 11:e1005204.
  21. Jacobs NT, Onuoha NO, Antia A, Antia R, Steel J, Lowen AC. 2019. Incomplete influenza A virus genomes are abundant but readily complemented during spatially structured viral spread. *bioRxiv*.
  22. Phipps KL, Ganti K, Jacobs NT, Lee C-Y, Carnaccini S, White MC, Manandhar M, Pickett BE, Tan GS, Ferreri LM, Perez DR, Lowen AC. 2020. Collective interactions augment influenza A virus replication in a host-dependent manner. *bioRxiv*.
  23. Phipps KL, Marshall N, Tao H, Danzy S, Onuoha N, Steel J, Lowen AC. 2017. Seasonal H3N2 and 2009 Pandemic H1N1 Influenza A Viruses Reassort Efficiently but Produce Attenuated Progeny. *J Virol* 91.
  24. Scholtissek C, Rohde W, Von Hoyningen V, Rott R. 1978. On the origin of the human influenza virus subtypes H2N2 and H3N2. *Virology* 87:13-20.
  25. Li KS, Guan Y, Wang J, Smith GJ, Xu KM, Duan L, Rahardjo AP, Puthavathana P, Buranathai C, Nguyen TD, Estoepangestie AT, Chaisingh A, Auewarakul P, Long HT, Hanh NT, Webby RJ, Poon LL, Chen H, Shortridge KF, Yuen KY, Webster RG, Peiris JS. 2004. Genesis of a highly pathogenic and potentially pandemic H5N1 influenza virus in eastern Asia. *Nature* 430:209-13.

26. Nelson MI, Viboud C, Simonsen L, Bennett RT, Griesemer SB, St George K, Taylor J, Spiro DJ, Sengamalay NA, Ghedin E, Taubenberger JK, Holmes EC. 2008. Multiple reassortment events in the evolutionary history of H1N1 influenza A virus since 1918. *PLoS Pathog* 4:e1000012.
27. Zhang X, Sun H, Cunningham FL, Li L, Hanson-Dorr K, Hopken MW, Cooley J, Long LP, Baroch JA, Li T, Schmit BS, Lin X, Olivier AK, Jarman RG, DeLiberto TJ, Wan XF. 2018. Tissue tropisms opt for transmissible reassortants during avian and swine influenza A virus co-infection in swine. *PLoS Pathog* 14:e1007417.
28. Brooke CB, Ince WL, Wrammert J, Ahmed R, Wilson PC, Bennink JR, Yewdell JW. 2013. Most influenza A virions fail to express at least one essential viral protein. *J Virol* 87:3155-62.
29. Diefenbacher M, Sun J, Brooke CB. 2018. The parts are greater than the whole: the role of semi-infectious particles in influenza A virus biology. *Curr Opin Virol* 33:42-46.
30. Buchholz UJ, Finke S, Conzelmann KK. 1999. Generation of bovine respiratory syncytial virus (BRSV) from cDNA: BRSV NS2 is not essential for virus replication in tissue culture, and the human RSV leader region acts as a functional BRSV genome promoter. *J Virol* 73:251-9.
31. Marshall N, Priyamvada L, Ende Z, Steel J, Lowen AC. 2013. Influenza virus reassortment occurs with high frequency in the absence of segment mismatch. *PLoS Pathog* 9:e1003421.
32. Tao H, Li L, White MC, Steel J, Lowen AC. 2015. Influenza A Virus Coinfection through Transmission Can Support High Levels of Reassortment. *J Virol* 89:8453-61.
33. Li ZN, Mueller SN, Ye L, Bu Z, Yang C, Ahmed R, Steinhauer DA. 2005. Chimeric influenza virus hemagglutinin proteins containing large domains of the Bacillus anthracis protective antigen: protein characterization, incorporation into infectious influenza viruses, and antigenicity. *J Virol* 79:10003-12.
34. Brochu-Lafontaine V, Lemay G. 2012. Addition of exogenous polypeptides on the mammalian reovirus outer capsid using reverse genetics. *J Virol Methods* 179:342-50.
35. White MC, Steel J, Lowen AC. 2017. Heterologous Packaging Signals on Segment 4, but Not Segment 6 or Segment 8, Limit Influenza A Virus Reassortment. *J Virol* 91.
36. Fodor E, Devenish L, Engelhardt OG, Palese P, Brownlee GG, Garcia-Sastre A. 1999. Rescue of influenza A virus from recombinant DNA. *J Virol* 73:9679-82.
37. Steel J, Lowen AC, Mubareka S, Palese P. 2009. Transmission of influenza virus in a mammalian host is increased by PB2 amino acids 627K or 627E/701N. *PLoS Pathog* 5:e1000252.
38. Boehme KW, Ikizler M, Kobayashi T, Dermody TS. 2011. Reverse genetics for mammalian reovirus. *Methods* 55:109-13.

39. Kanai Y, Komoto S, Kawagishi T, Nouda R, Nagasawa N, Onishi M, Matsuura Y, Taniguchi K, Kobayashi T. 2017. Entirely plasmid-based reverse genetics system for rotaviruses. *Proc Natl Acad Sci U S A* 114:2349-2354.
40. Virgin HWt, Bassel-Duby R, Fields BN, Tyler KL. 1988. Antibody protects against lethal infection with the neurally spreading reovirus type 3 (Dearing). *J Virol* 62:4594-604.
41. Furlong DB, Nibert ML, Fields BN. 1988. Sigma 1 protein of mammalian reoviruses extends from the surfaces of viral particles. *J Virol* 62:246-56.
42. Zhou B, Donnelly ME, Scholes DT, St George K, Hatta M, Kawaoka Y, Wentworth DE. 2009. Single-reaction genomic amplification accelerates sequencing and vaccine production for classical and Swine origin human influenza A viruses. *J Virol* 83:10309-13.

### **Chapter III. Mammalian orthoreovirus reassortment proceeds with little constraint on segment mixing**

Megan R. Hockman<sup>1</sup>, Nathan T. Jacobs<sup>1</sup>, Bernardo A. Mainou<sup>2#</sup>, Katia Koelle<sup>3</sup> and Anice C. Lowen<sup>1\*</sup>

<sup>1</sup> Department of Microbiology and Immunology, Emory University School of Medicine, Atlanta, GA, 30322, USA

<sup>2</sup> Department of Pediatrics, Emory University School of Medicine, Atlanta, GA, 30322, USA

<sup>3</sup> Department of Biology, Emory College of Arts and Sciences, Atlanta, GA, 30322, USA

#Current address: Centers for Disease Control and Prevention, Atlanta, GA, 30329, USA

\*anice.lowen@emory.edu

The work of this chapter was submitted for publication in the Journal of Virology in October 2021.

## **Abstract**

Segmentation of viral genomes gives the potential for genetic exchange within co-infected cells.

However, for this potential to be realized, co-infecting genomes must mix during the viral lifecycle. The efficiency of reassortment in turn dictates its potential to drive evolution. The opportunity for mixing within co-infected cells may vary greatly across virus families, such that the evolutionary implications of genome segmentation differ as a result of core features of the viral lifecycle. To investigate the relationship between viral replication compartments and genetic exchange, we quantified reassortment in mammalian orthoreovirus (reovirus).

Reoviruses carry a 10-segmented, double-stranded RNA genome, which is replicated within proteinaceous structures termed inclusion bodies. We hypothesized that inclusions impose a barrier to reassortment. We quantified reassortment between wild-type (*wt*) and variant (*var*) reoviruses that differ by one nucleotide per segment. *Wt/var* systems in both T1L and T3D backgrounds revealed frequent reassortment without bias towards particular genotypes.

However, reassortment was more efficient in the T3D serotype. Since T1L and T3D viruses exhibit different inclusion body morphologies, we tested the impact of this phenotype on reassortment. In both serotypes, reassortment levels did not differ by inclusion morphology.

Reasoning that the merging of viral inclusions may be critical for genome mixing, we then tested the effect of blocking merging. Reassortment proceeded efficiently even under these conditions.

Our findings indicate that reovirus reassortment is highly efficient despite the localization of many viral processes to inclusion bodies, and that the robustness of this genetic exchange is independent of inclusion body structure and fusion.

## **Importance**

Quantification of reassortment in diverse viral systems is critical to elucidate the implications of genome segmentation for viral evolution. In principle, genome segmentation offers a facile means of genetic exchange between coinfecting viruses. In practice, there may be physical

barriers within the cell that limit mixing of viral genomes. Here, we tested the hypothesis that localization of the various stages of the mammalian orthoreovirus lifecycle within cytoplasmic inclusion bodies compartmentalizes viral replication and limits genetic exchange. Contrary to this hypothesis, our data indicate that reovirus reassortment occurs readily within co-infected cells and is not strongly affected by the structure or dynamics of viral inclusion bodies. We conclude that the potential for reassortment to contribute to reovirus evolution is high.

## **Introduction**

Mammalian orthoreovirus (reovirus) is a member of the *Reoviridae* family with a 10-segmented double-stranded RNA (dsRNA) genome. The segmented nature of its genome gives rise to the potential for reassortment, the process by which segments from co-infecting parental viruses are exchanged and packaged together to yield progeny bearing novel genotypes. Along with mutation, reassortment is an important source of genetic diversity, making the potential implications of reassortment for viral evolution great. Reassortment can bring together beneficial mutations from genetically distinct parental viruses, relieving clonal interference, and resulting in progeny with enhanced fitness (1, 2). Similarly, reassortment allows purging of deleterious mutations that could otherwise prevent positive selection from acting on advantageous mutations elsewhere in the genome (3, 4). Cumulatively, reassortment allows selection to act more efficiently and can thereby enable the evolution of viruses with enhanced replicative potential, an expanded host range, or more efficient immune avoidance mechanisms.

A comprehensive understanding of the implications of reassortment for viral evolution depends on an understanding of how readily reassortment occurs during viral co-infection. Influenza A virus reassortment is highly efficient due to a reliance on co-infection for productive replication (5-7). Furthermore, the influenza A virus lifecycle appears to allow free segment mixing within co-infected cells, which may facilitate complementation and reassortment. Unlike influenza A virus, reovirus replicates within virus-derived inclusion bodies (inclusions) (8-10)

that may impose a physical barrier to segment mixing. Examination of reovirus reassortment therefore presents an opportunity to broaden our understanding of the relationship between viral genome segmentation and diversification through genetic exchange. Barriers to viral mixing within the cell may strongly limit reassortment and, in turn, minimize the impact of genome segmentation on viral evolution.

Reovirus replication occurs within the host cell cytoplasm, with much of the lifecycle confined to proteinaceous viral inclusions (11). The  $\mu$ NS protein is a major structural component of inclusions: expression of this protein alone is sufficient for formation of inclusion-like objects. However, more complex structures are formed in the context of infection, with recruitment of many viral and cellular components to inclusion bodies (12-16). Of note, rough endoplasmic reticulum membranes and ribosomes are recruited, which may remove the need for viral mRNAs to enter the cytoplasm to be translated. Translation of viral mRNA has been observed at the periphery of viral inclusions (15, 17, 18).

In most serotypes, viral inclusions exhibit filamentous morphology due to interactions between the viral  $\mu$ 2 protein and the host cell microtubule network. Additional interactions between  $\mu$ 2 and the inclusion-forming  $\mu$ NS protein lead to the characteristic filamentous inclusion morphology, which co-localize with microtubules (8, 9, 19). By contrast, the T3D serotype generates globular inclusions due to a single point mutation in the  $\mu$ 2 gene resulting in a proline substitution at position 208 (S208P) (9). This amino acid change abrogates  $\mu$ 2's interaction with microtubules and causes more frequent misfolding and ubiquitination of the  $\mu$ 2 protein (20).

Reovirus inclusions coalesce during infection (21, 22). Inclusions in another dsRNA virus, infectious bursal disease virus, also merge together over time and this process has been shown to yield mixed inclusion bodies within co-infected cells (23). If viral mRNAs are sequestered within inclusions (14), merging may serve as a primary source of genetic exchange. It is not known whether inclusion morphology (dictated by the  $\mu$ 2 protein) plays a role in

segment movement. T1L and T3D viruses represent tractable systems in which to explore this possibility, as a single point mutation is sufficient to change inclusion morphology from globular to filamentous, and *vice versa*.

Here, we sought to quantify reovirus reassortment and evaluate the role of viral inclusions in determining reassortment frequency. Reovirus reassortment was quantified in a previously developed fitness-neutral system that uses homologous parental strains (24). To compare baseline reassortment frequencies between serotypes, reassortment was quantified in both T1L and T3D viruses. Reassortment was efficient in both systems, but more so in T3D. The impact of inclusion morphology was also investigated in each serotype. Alteration of inclusion morphology to either globular (in the T1L system) or filamentous (in the T3D system) had minimal impact on reassortment, indicating that morphology is not an important determinant of genetic exchange. To investigate the role of inclusion merging in reassortment, cells were treated with nocodazole, which has been shown to block the fusion of inclusions (22). Reassortment levels were not markedly affected by nocodazole treatment, suggesting that inclusion merging plays a minimal role in facilitating genetic exchange.

## **Results**

### **Quantification of Reovirus Reassortment**

Reassortment between divergent viruses often leads to the production of attenuated progeny due to incompatibilities between genome segments and/or proteins from different parental viruses (25). Decreased fitness may cause these progeny to be removed from the population by negative selection, leading to underrepresentation of reassortment frequencies. To quantify reassortment in the absence of segment mismatch, we designed well-matched parental viruses for co-infection. We reported this method previously (24, 26) and have applied it here to both T1L and T3D serotypes. Briefly, silent point mutations were introduced into each wild-type (*wt*) virus to generate a variant (*var*) strain that differs from *wt* by one nucleotide per gene segment. We previously showed that there is no significant difference in the replicative

fitness of T3D*wt* and T3D*var* in cell culture (24). Equivalent analysis was performed here in the T1L system: T1L*wt* and T1L*var* exhibited equivalent titers over the course of a 36-hour infection (Figure 1A). These results confirm that the genotypically similar *wt* and *var* viruses are also phenotypically comparable, as intended. Owing to the silent nature of the mutations introduced, we expect this phenotypic similarity between parental viruses to extend to reassortant progeny. To ensure that a single nucleotide polymorphism was sufficient to distinguish the gene segments of *wt* and *var* viruses, high-resolution melt analysis was performed on qRT-PCR amplicons of the viral RNAs. In this approach, amplicons are heated gradually in the presence of a double-strand intercalating dye, such as EvaGreen. This gradual heating allows precise measurement of the amplicon's melting point, the temperature at which the amplicon separates into two DNA strands (27). The melting properties of each *var* segment differed from its corresponding *wt* segment, indicating that the introduced polymorphisms were sufficient to identify the parental origin of each segment (Figure 1B; (24)).

To quantify reassortment in each background, *wt* and *var* viruses were mixed in equal proportions and diluted to a range of virion concentrations. L929 cells, which are highly permissive to reovirus infection, were inoculated under synchronized, single-cycle conditions. Synchronization is achieved by allowing viruses to attach at 4° C prior to triggering entry by warming to 37° C; this process narrows the time frame in which infection occurs such that co-infections are essentially simultaneous. Single cycle conditions prevent the propagation of viral progeny arising from the initial inoculation, which in turn ensures that viruses sampled are direct progeny of the parental *wt* and *var* viruses. At 24 hours post-inoculation (hpi), progeny viruses were collected for genotyping of clonal isolates and analysis of reassortment frequencies. The resultant data in the T1L (Figure 2A) and T3D (Figure 2B) backgrounds revealed that reassortment increased with increasing MOI and reached high levels, with greater than 80% of progeny carrying reassortant genotypes at the highest MOIs tested. To more formally assess reassortment efficiency, we compared observed results to the prediction of a simple theoretical

model that assumes a random distribution of viruses across cells and perfectly random mixing of segments within co-infected cells. T3D reassortment was similar to model predictions, consistent with robust segment exchange in co-infected cells. However, observed T1L reassortment was less efficient than predicted by the model and significantly less efficient than that of T3D ( $P=0.0009$ , mixed-effects analysis).

### **Reovirus segments assort randomly in co-infected cells**

Quantification of the proportion of progeny that are reassortant (as reported above) is informative of the efficiency of segment mixing, but does not exclude the possibility that interactions between segments may bias reassortment towards the production particular genotypes. To determine whether interactions between segments favor the production of certain reassortant genotypes over others, we quantified pairwise associations between segments. The pairwise associations (indicated by  $r^2$ ) are a measure of segment linkage, with high  $r^2$  values indicating that the two segments considered are found together in the same virus more often than would be expected by chance. If frequencies of viral co-infection and segment mixing are high, reassortment can break segment linkage; however, even under conditions conducive to reassortment, physical or functional interactions between segments may constrain this process and lead to maintenance of linkage. Because the co-infecting viral genomes of *wt* and *var* viruses are highly homologous, we predicted that segment exchange would occur without genetic constraint.

To test our prediction, the genotypes of progeny from each viral population were analyzed to quantify pairwise associations between segments at each MOI. Specifically,  $r^2$ , was calculated for each pair of segments (e.g., M2 and S3) to quantify the extent to which both segments were derived from the same parental strain. At low MOIs,  $r^2$  was high for most segment pairs, but these associations decayed as MOI increased (Figure 3). Importantly, at high MOIs, when co-infection is expected to be common, a segment derived from a given parental strain co-occurred with segments from either parent with roughly equal frequency and  $r^2$  values

were therefore low. This result indicates a lack of pairwise association between segments under conditions where reassortment is abundant. Thus, when considering homologous co-infecting viruses, reovirus reassortment efficiently breaks genetic linkages among the ten gene segments. Given these data, we conclude that segments are assorted independently.

### **Inclusion morphology has minimal impact on reassortment**

Based on the observation that reassortment is more efficient in T3D than in T1L viruses, we hypothesized that globular inclusions (like those of T3D) are more conducive to segment mixing within the cell than filamentous inclusions (like those of T1L). We reasoned that viral inclusions are likely to impose physical barriers to segment mixing, reducing the efficiency of reassortment relative to a cellular infection in which segments mix freely without physical barriers. Furthermore, inclusions that differ in structure could vary in their capacities to restrict reassortment. To directly test the impact of inclusion morphology, reassortment efficiency was quantified in both reovirus serotypes using targeted mutants designed to alter inclusion morphology. Consistent with most reovirus serotypes, the T1L virus generates filamentous inclusion bodies which have been shown to co-localize with the microtubule network (19). We confirmed that this morphology was adopted using confocal microscopy (Figure 4A). A single amino acid change of P208S in the  $\mu 2$  protein abrogates its interaction with microtubules, resulting in the formation of globular inclusion bodies (9). Generation of a T1L virus bearing this polymorphism successfully altered inclusion morphology (Figure 4A). The converse mutation was introduced in T3D, which normally forms globular inclusions. The inclusion morphologies of T3D (globular) and T3DS208P (filamentous) were confirmed using confocal microscopy (Figure 4B).

Reassortment frequencies did not appreciably differ between T1L and T1LP208S at any MOI tested (Figure 4C). However, T3DS208P, which formed filamentous inclusions, exhibited consistently lower levels of reassortment compared to its globular counterpart T3D (Figure 4D). Therefore, changing T3D inclusions from globular to filamentous moderately suppressed

reassortment, but the converse change in T1L did not increase reassortment as hypothesized. Given these inconsistent outcomes, we reasoned that inclusion morphology may not be a primary determinant of reassortment efficiency. Rather, mutation of  $\mu 2$  position 208 may have differentially affected virus infectivity in the T1L and T3D backgrounds, in turn altering reassortment at comparable multiplicities of infection.

To evaluate the infectivity of the viruses tested, co-infected cells stained for the viral structural protein  $\sigma 3$  were analyzed by flow cytometry. The T1L wild-type and  $\mu 2$  mutant viruses showed comparable levels of infection, with the P208S mutation causing a 1.06-fold increase in the proportion of cells infected. Notably, however, the S208P mutation in the T3D background had a marked effect on infectivity, leading to a 0.48-fold change in the proportion of cells infected (Figure 4E).

To determine the contribution of infectivity, rather than inclusion morphology, to observed differences in reassortment between T3D and T3DS208P, we evaluated the proportion of reassortant progeny viruses relative to the proportion of cells infected (Figure 4F). When analyzed in this way, reassortment levels observed for T3D and T3DS208P were similar. Comparison of T1L and T1LP208S reassortment using this approach also showed little difference. Thus, at a given level of infection, filamentous and globular variants of a given serotype display comparable levels of reassortment. We therefore conclude that the frequency of reassortment in reovirus infected cells is not strongly modulated by inclusion morphology.

### **Efficiency of reovirus infection**

To better understand the relationship between MOI and infectivity, the  $\sigma 3$ -positive cell population was analyzed as a function of MOI. The Poisson expectation for the proportion of cells infected was used as a baseline for comparison and, relative to this expectation, all viruses exhibited markedly lower levels of infection (Figure 5A).

The disparity between observed and expected infection levels at a given MOI raised the possibility that not all virus particles successfully reach cells during the attachment period. To

address this possibility, we conducted a series of infections across a range of MOIs, and quantified unattached viruses remaining in the liquid inoculum at the end of the attachment period. Specifically, remaining liquid inoculum was pooled with washes performed following attachment, and viruses in the resultant pools were titered by plaque assay. The average proportion of inoculum virus detected in this residual sample was  $0.594 \pm 0.09$  in T3D, and  $0.593 \pm 0.1$  in T1L (95% CI), with no clear effect of MOI. Thus, the MOI accounting for infection was approximately 40% of that added to the cells. Adjusting the Poisson expectations based on this information did not change the overall conclusion that measured infection of all viruses is markedly lower than the expectation (Figure 5A). This result suggests that either 1) the flow cytometry assay detects only a subset of infected cells; or 2) a high proportion of viruses fail to initiate productive infection, despite successful attachment to the cell monolayer. We favor the former interpretation based on the observed relationship between MOI and total viral output at 24 h post-inoculation: although the detected proportion of cells infected increases very gradually over the low MOI range, viral yield increases rapidly (Figure 5B). For this reason, we did not generate predictions of reassortment frequency based on measured proportions of infected cells.

### **Disruption of microtubules does not impact reovirus genetic exchange**

To further investigate the role of inclusions in defining reassortment potential, we treated infected cells with nocodazole, which disrupts the microtubule network and has been shown to inhibit inclusion body fusion (22). Nocodazole was added to L929 cells infected with T3D and T3DS208P at 6 hpi and inclusions were visualized at 21 hpi using confocal microscopy (Figure 6A and 6B). Addition of nocodazole resulted in small, dispersed inclusions in both T3D and T3DS208P infected cells, as expected under conditions where inclusion merging is inhibited (22). To test the contribution of inclusion merging to reassortment, we then quantified reassortment in the presence of nocodazole (Figures 6C and 6D). These results show that addition of nocodazole minimally impacted reassortment efficiency in both T3D and

T3DS208P. We conclude that inclusion merging was not required for reassortment regardless of inclusion morphology.

## **Discussion**

Our results show that reovirus reassortment occurs readily in co-infected cells, with efficient assortment of all ten gene segments observed under conditions conducive to cellular co-infection. Altering of inclusion morphology did not affect reassortment frequencies in either T1L or T3D backgrounds, indicating that reassortment efficiency is not dependent on inclusion morphology. Furthermore, addition of nocodazole, which has been shown to inhibit fusion of inclusion bodies and resulted in the formation of small, dispersed inclusions in our experiments, did not result in decreased reassortment. Coalescence of inclusions may therefore not be required for genetic exchange between co-infecting reoviruses.

Previous studies using temperature-sensitive T3D mutant viruses provided clear evidence that reovirus gene segments can reassort, allowing reconstitution of a wild type genotype from parental viruses that carried distinct temperature-sensitive mutations on differing segments. These studies could also be interpreted quantitatively and showed that wild type (that is, non-temperature-sensitive) progeny viruses occurred with a frequency of 3-8% when co-infections were carried out at MOIs ranging from 0.1 to 100 PFU/cell (28, 29). Importantly, these results relied on quantification of reassortment between only the two temperature-sensitive segments. Extrapolating these findings to consider reassortment involving any of the ten segments yields an estimate of 6–16% reassortment. By comparison, our results indicate that T3D reassortment is more efficient, with as many as 25–100% of progeny bearing reassortant genomes. Reasons for this difference are not clear, since the same virus serotype and cell line were used.

Equivalent quantification of reassortment in T1L (which has not been previously evaluated) revealed a disparity in reassortment between the serotypes. When comparing

reassortment levels to mathematical predictions that assume free mixing of segments within cells and random distribution of infecting viruses, T3D reached predicted levels of reassortment while T1L remained below expectations. These differences between the serotypes were not explained by inclusion body morphology. Serotype-specific differences in cellular responses to infection, primarily in activation of cell-intrinsic antiviral responses and induction of cell death, have been observed. Compared to T1L, T3D is a more potent activator of type I interferons (30), and more frequently causes cell death by both apoptosis and necroptosis (31, 32). Infection with T3D also results in more frequent arrest of infected cells in the G<sub>2</sub>/M phase of the cell cycle (33). It is unclear whether the differences in reassortment relate to these known variations in reovirus interactions with the host cell, or whether they are due to as-yet unknown features of the virus' biology.

In influenza A virus, high levels of reassortment result from a reliance of the virus on multiple infection for productive replication (5-7): owing to the prevalence of incomplete viral genomes, the probability of a cell producing viral progeny increases with the number of co-infecting viruses, which in turn augments the proportion of progeny viruses that are reassortant. Our results give insight into whether reovirus has a similar reliance on multiple infection. Figure 2 indicates that reovirus reassortment is consistent with (T3D) or below (T1L) our model predictions. This model assumes a linear relationship between viral input and viral output; no synergistic effect of co-infection is incorporated. As such, our data suggest that a reliance on multiple infection for productive replication is unlikely to apply in the reovirus system. Extending this logic, our results suggest that cells infected by even a single reovirus particle typically support replication of all ten gene segments.

Levels of reassortment are also reliant on the distribution of viruses into target cells. The simple model presented herein assumes a random, Poisson distribution and our data are generally consistent with this assumption. Delivery of multiple virus particles to a cell through various mechanisms of collective dissemination would be expected to increase reassortment

(assuming the collectives include a mixture of *wt* and *var* particles). For example, reovirus aggregation (34-37), delivery of multiple virions inside extracellular vesicles (observed in rotavirus (38)), or scaffolding of multiple virions onto bacterial components (39, 40) could facilitate co-infection. While observed levels of infection in our experiments were lower than the Poisson expectation based on MOI, the shape of the infection curve was consistent with a random distribution. Additionally, the infection conditions employed in our experiments, using gradient-purified viruses, did not favor collective virus dissemination. Finally, the levels of reassortment observed either approximate (T3D) or are somewhat lower than (T1L) those predicted by our model, whereas collective dissemination would be expected to promote cellular co-infection and thus increase reassortment. Therefore, our data indicate that viral aggregates or other groupings were not a major factor driving reassortment in our experiments.

We hypothesized that inclusion coalescence was an important source of genetic mixing that led to the high levels of reassortment observed. Coalescence has been observed in the reovirus system (22), and can result in the formation of mixed inclusion bodies containing protein from both viruses (23). Blocking inclusion merging by disrupting microtubules with nocodazole presented a tractable way to test the impact of merging on reassortment. While large inclusions did not form, suggesting a lack of merging, reassortment levels were unchanged. We therefore conclude that merging may not be required for genetic exchange and suggest that segments may be exchanged as a result of viral mRNA transport through the cytoplasm.

Taken together, our data show that reovirus reassortment is more efficient than expected from the compartmentalized nature of its replication and this compartmentalization may not substantially influence reassortment frequency. Thus, the potential for reassortment to drive reovirus evolution is not markedly limited by barriers acting within the cell. Rather, reovirus genome segmentation affords ample opportunity for genetic exchange within co-infected cells.

## Materials and Methods

### Experimental Methods

#### *Viruses and Cells*

Spinner-adapted L929 cells (Terry Dermody, University of Pittsburgh) were grown at 37 °C in Joklik's modified MEM supplemented with 5% FBS, 2 mM L-Glutamine, penicillin and streptomycin (PS), and 0.25 mg/mL amphotericin B, termed SMEM. BHK-T7 cells (41) were maintained in DMEM supplemented with 5% FBS, 2 mM L-Glutamine, PS, and 1 mg/mL G418 at 37° C. Cells were tested monthly for mycoplasma and discarded if found to be positive. Parental T1L (Accession SRX6802328) and T3D (Accession SRX6802327) viruses were generated by reverse genetics (42) and were deep sequenced previously (43). Variant (*var*) T1L and T3D viruses were designed as described previously (24). As previously reported, point mutations to generate T3D *var* were: L1 C612T, L2 C853T, L3 G481A, M1 C919T, M2 A650G, M3 T702C, S1 G312A, S2 A438G, S3 T318C, and S4 C383T. Point mutations to generate T1L *var* were: L1 T606C, L2 T852C, L3 A481G, M1 T919C, M2 G650A, M3 C702T, S1 A313G, S2 C426T, S3 C318T, and S4 T383C. Additional point mutations were made at nucleotide 635 in the M1 segment (T1L C635T, T3D T635C) of both serotypes to alter inclusion morphology as shown previously (9). These viruses were generated by reverse genetics in BHK-T7 cells and propagated in L929 cells for three passages prior to Vertrel XF extraction and purification on a cesium chloride gradient (44).

#### *Viral Replication Kinetics*

L929 cells were infected with purified *wt* and *var* viruses of the T1L and T3D serotypes using synchronized, single-cycle conditions. At the time of infection, cells were placed on ice and washed once with 1X PBS. 100 µL of virus inoculum in OPTI-MEM at an MOI of 10 PFU/cell was added to each well. Cells were placed at 4°C and virus was attached for 1 h, rocking every 10 minutes. Keeping cells cold ensured that virus infection is synchronized, with all attached viruses entering cells simultaneously upon warming. After attachment, cells were placed back on

ice and washed 3 times with cold 1X PBS. Warm SMEM was added to cells which were then placed at 37°C. At each time point, one plate was removed from incubation and stored at -80°C. At 4 hpi, warm SMEM containing 20 mM NH<sub>4</sub>Cl (T3D) (24) or 4 mM E64-d protease inhibitor (T1L) was added to each well in order to limit further rounds of replication. Samples were titered by plaque assay on L929 cells as described previously (45).

### *Co-Infections*

Co-infections were performed using single-cycle conditions as described above. 100 µL of an equal parts mixture of *wt* and *var* viruses in OPTI-MEM was added to cells seeded in 12 well dishes at a range of MOI's. Cells were incubated for 24 hours in 1 mL SMEM. Warm SMEM containing 4 mM E64D was added to T3D infections at 4 hpi and T1L infections at 7 hpi. To determine the impact of nocodazole on reassortment, 10 µM nocodazole was added to wells infected with T3D viruses at 6 hpi. Co-infection plates were placed directly at -80° C for 3X freeze-thaw cycles. Well contents were transferred to 1.5 mL Eppendorf tubes and stored at -80° C.

### *Flow cytometry to quantify infected cells*

Cells were harvested from 12-well plates by the addition of 100 µL trypsin (Corning) and, once they were detached, 900 µL of FACS buffer (1X PBS with 2% FBS). Cells were transferred to 1.5 mL tubes on ice and washed twice in FACS buffer. Fixation, permeabilization, and staining were performed according to the BD Cytofix/Cytoperm protocol. A 15-minute blocking step using BD rat anti-mouse CD16/CD32 Fc block was included. Infected cells were stained with a mouse monoclonal anti-σ3 antibody (clone 10C1) at a concentration of 1 µg/mL for 30 minutes at 4°C. Cells were washed twice, and an AlexaFluor-647 conjugated donkey anti-mouse secondary antibody (Invitrogen) was added at a 1:1000 dilution. Cells were washed three more times and then resuspended in FACS buffer for analysis.

Data was collected on a BD LSR II Flow cytometer running FACS Diva software. A minimum of 50,000 events was collected for each sample. Analysis and gating were performed using FlowJo

(v10.1). A gate was included to select single cells. Further gating selected infected cells based on positivity greater than that of an antibody stained, mock-infected control.

#### *Wash Titers*

A dedicated set of infections was performed to determine the amount of virus that did not attach during co-infections and was subsequently washed away. L929 cells seeded in 6-well dishes were infected at MOIs of 0.1, 1.0, 10, and 100 PFU/cell following the synchronization protocol noted above. The supernatant was collected and pooled with 3X 200  $\mu$ L washes of cold 1X PBS. Pooled supernatant and washes were titered using a plaque assay, and the percentage of virus lost during attachment was determined based on input virus (MOI  $\times$  Number of Cells Infected).

#### *Quantification of Reassortment*

To obtain clonal isolates, plaque assays were performed in L929 cells with supernatant from *wt/var* co-infections. Well-separated plaques were picked into 120  $\mu$ L of PBS in 96-well assay blocks. A total of 32 plaques were picked for each sample at each MOI. Samples were stored at -20 °C or used immediately for RNA extraction.

RNA extraction was performed using the Zymo *Quick*-RNA Viral Kit I-96 well format RNA extraction kit according to the manufacturer's protocol. RNA was eluted in 40  $\mu$ L water into a MicroAmp Optical 96-well reaction plate (Applied Biosystems, N8010560).

Reverse transcription was performed in 96-well plates using Maxima reverse transcriptase (Fermentas), random hexamer primers (Thermo), and 12.8  $\mu$ L of extracted RNA template. qPCR was performed in 385-well plates (BioRad, HSP3805). 3  $\mu$ L of a master mix containing 1X Precision Melt Supermix (BioRad) and 0.4  $\mu$ M of a mixture of forward and reverse primers was mixed with 2  $\mu$ L of cDNA for a total reaction volume of 5  $\mu$ L. qPCR results were analyzed using Bio-Rad CFX Manager software, and melt curves were analyzed using Bio-Rad Precision Melt Analysis software.

#### *Immunofluorescence*

To analyze viral inclusion morphology, infected cells were visualized using immunofluorescence and confocal microscopy.

L929 cells were seeded onto Nunc Lab-Tek II single chambered slides (Thermo) coated with human placenta collagen. The next day, cells were infected at an MOI of 5 PFU/cell of virus. Nocodazole validation was performed using synchronized, multi-cycle conditions (attachment at 4°C, no E64D added) and filamentous/globular inclusion morphologies were validated using single-cycle conditions noted in the *Viral Replication Kinetics* section.

At 20 hpi (nocodazole) and 18 hpi (inclusion morphology), cells were washed 3 times with 1X PBS and fixed for 15 minutes at room temperature with 4% paraformaldehyde. Fixed cells were washed 3 more times with 1X PBS and permeabilized for 10 minutes with 0.2% Triton-X 100 in 1X PBS. Cells were blocked for 30 minutes with block buffer (1X PBS with 0.1% Tween-20 and 1% BSA), then guinea pig anti-σNS polyclonal antibody (gift from Bernardo Mainou) at a 1:5000 dilution in 1% BSA in 1X PBS was added to cells and allowed to incubate for 2 hours at room temperature. Cells were washed 3 times in 1X PBS, and Alexa Fluor 488-conjugated goat anti-guinea pig IgG H+L (Jackson ImmunoResearch, 106-545-003) was added at a 1:2500 dilution in 1% BSA in 1X PBS and incubated for 1 hour at room temperature.

Cells were washed three times in 1X PBS, and 4 mM DAPI diluted in nuclease free water was added to cells which were incubated for 4 minutes. Cells were washed 3 more times in 1X PBS and mounted with VectaShield mounting medium.

Cells were visualized using an Olympus FV1000 Inverted Confocal Microscope with an Olympus Plan Apo 100X 1.45 NA lens. DAPI fluorophore was excited using the 405 laser and Alexa-488 fluorophore was excited using the 488 laser line from an Argon laser. Kalman averaging was employed to reduce noise. Images were obtained using the Olympus Fluoview v4.2. software. Z-series optical sections were collected, with 13-24 slices at thicknesses ranging from 0.3 μM to 0.6 μM.

## Computational Methods

### *Estimating the Expected Proportion Infected Cells*

The expected proportion of infected cells at a given multiplicity of infection (MOI) was determined using a Poisson distribution.

$$\text{Proportion Infected Cells} = 1 - e^{-\lambda}$$

Here,  $\lambda$  represents the mean of the distribution and is equal to MOI.

### *Input vs. Output Relationship*

The observed relationship between viral input and output appears linear (Figure 5B). As such, we let the number of output viral progeny from a cell infected with  $i$  virions be given by:

$$c(i) = k \times i$$

where  $k$  is the number of viral progeny produced by a virion that has entered a cell. Total viral output from a population of  $N$  cells is then determined using the formula:

$$v(i) = \sum_i [P(i) \times c(i) \times N]$$

$P(i)$ , the probability that a cell has undergone entry of  $i$  virions, is given by a Poisson distribution parameterized with mean given by the MOI  $\lambda$ , evaluated at  $i$ .

### *Reassortment Prediction*

To model reassortment, the virus population must be split into two groups which are capable of co-infection. Reassortment requires co-infection to occur, and splitting the population into wild-type and variant viruses allows for this requirement to be taken into account.

The total number of virus particles that are produced at MOI  $\lambda$  is determined by multiplying the sum of the probabilities of  $i$  and  $j$  wild-type and variant viruses entering a cell, respectively, by the predetermined input/output relationship:

$$\sum_i \sum_j P(i)P(j)v(i+j)$$

Probabilities  $P(i)$  and  $P(j)$  were determined using Poisson expectations above.

To calculate the number of reassortant viruses, we first can write out the probability that a progeny virus from a cell will be reassortant if  $i$  wt and  $j$  var virions entered the cell. With the probability that a progeny virus will have all 10 gene segments be wild-type being given by  $(i/(i+j))^{10}$  and the probability that a progeny virus will have all 10 gene segments be var being given by  $(j/(i+j))^{10}$ , the probability that a progeny virus will be a reassortant genotype is given by:

$$\left[ 1 - \left( \frac{i}{i+j} \right)^{10} - \left( \frac{j}{i+j} \right)^{10} \right]$$

The final form of the equation to calculate the proportion of reassortant progeny is the number of reassortant viruses divided by the total number of viruses that emerge from the infection:

$$\frac{\sum_i \sum_j P(i)P(j) \left[ 1 - \left( \frac{i}{i+j} \right)^{10} - \left( \frac{j}{i+j} \right)^{10} \right] v(i+j)}{\sum_i \sum_j P(i)P(j)v(i+j)}$$

#### *Analysis of Pairwise Associations Between Segments*

To quantify non-random association of *wt* and *var* segments during reassortment, the Pearson correlation coefficient was determined for each pair of segments at each MOI using the formula:

$$r = \frac{\sum(x - m_x)(y - m_y)}{\sqrt{\sum(x - m_x)^2 \sum(y - m_y)^2}}$$

Where, summed across all progeny plaques that were genotyped in a sample,  $x$  is the genotype of the first segment in the pair of segments considered (e.g., M2; 1 = *wt*, 0 = *var*),  $y$  is the genotype of the second segment in the pair (e.g., S3; 1 = *wt* 0 = *var*),  $m_x$  is the proportion of first segments in the sample that are *wt*, and  $m_y$  is the proportion of second segments that are *wt*.

Each  $r$  value was squared to convert the correlation to an  $r^2$  measure.

### **Acknowledgments**

This work was funded by the National Institutes of Health through RO1 AI146260. The project was furthermore supported in part by the Emory University Integrated Cellular Imaging Core and the Emory Flow Cytometry Core (EFCC). Both cores are part of the Emory Integrated Core Facilities (EICF) and are subsidized by the Emory University School of Medicine. Additional support was provided by the Center for Georgia Clinical & Translational Science Alliance of the National Institutes of Health under Award Number UL1TRO02378. The content is solely the responsibility of the authors and does not necessarily reflect the official views of the National Institutes of Health.

## Figures and Tables

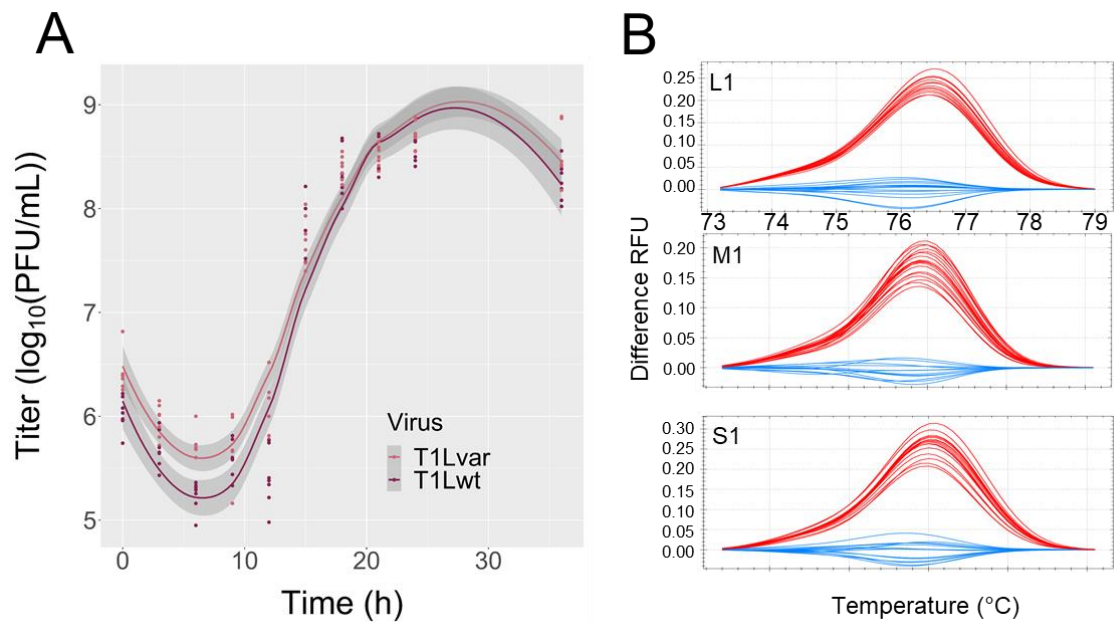


**Figure 1: T1L *wt* and *var* replicate to equivalent titers and can be differentiated using high-resolution melt analysis.** Single-cycle replication of T1L *wt* and *var* viruses was evaluated over a period of 36 hours (A). Plaques from this time course were then genotyped using high-resolution melt analysis. Melt curves were generated for each segment and compared to *wt* and *var* controls. Representative melt curves are shown (B). Difference in relative fluorescent units (RFU) is indicated on the y-axis.

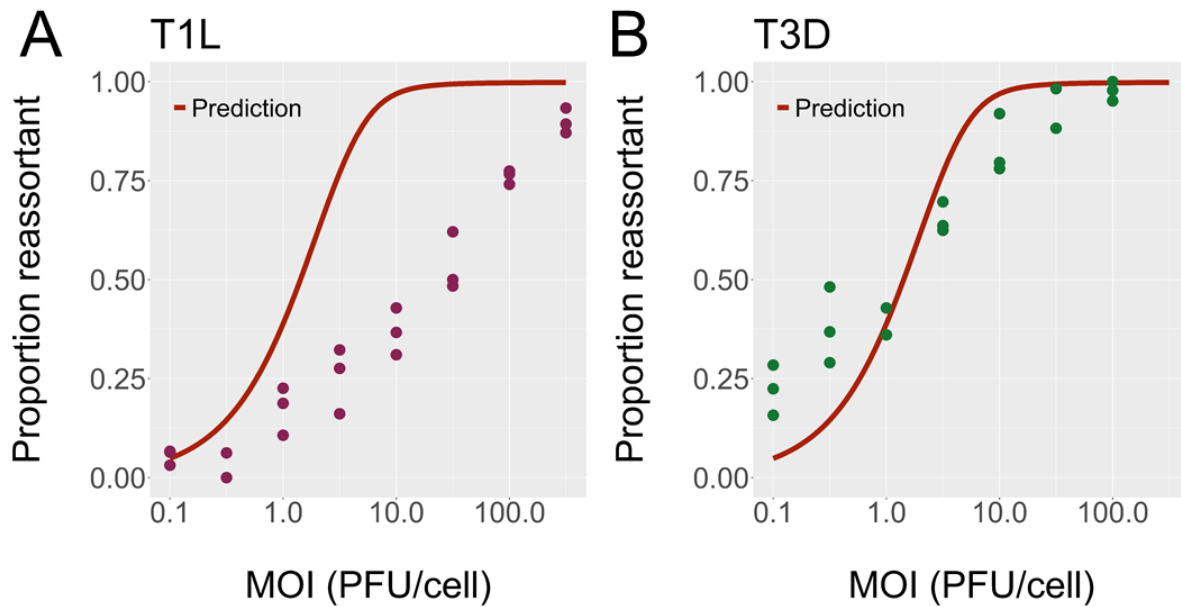


**Figure 2: Reovirus reassortment occurs frequently at high MOI and is more efficient in T3D than in T1L.** Reassortment between *wt* and *var* forms of the T1L (A) and T3D (B) strains of reovirus was quantified at a range of MOIs. Infections were performed in triplicate at each MOI. The proportion of progeny with any reassortant genotype is plotted against the MOI (PFU/cell). Experimental data are compared to a theoretical prediction that assumes random distribution of virus particles across cells and perfectly efficient mixing of gene segments in infected cells.

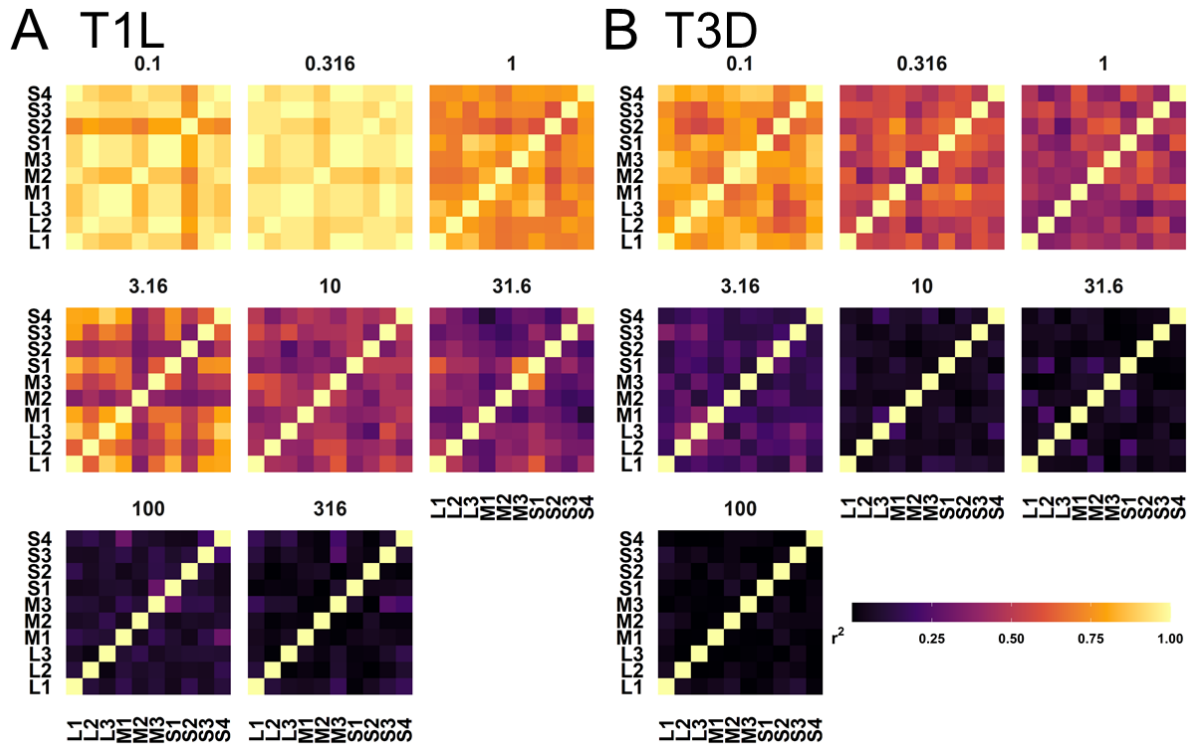


**Figure 3: Under high MOI conditions, there is little pairwise association between gene segments.** Genotypes of progeny viruses sampled from wt/var co-infections were analyzed to quantify pairwise associations between segments.  $r^2$  values indicating the extent of linkage between segments are shown. Each genome segment is shown on both the x and y axes, with blocks of color indicating the magnitude of  $r^2$ . Higher  $r^2$  values indicate an increased probability that both genome segments in a clonal isolate share the same parental genotype. Yellow coloration indicates a strong association, while purple indicates a weak or absent association. Results from co-infections with T1L *wt* and *var* (A), or T3D *wt* and *var* (B), are shown for each multiplicity of infection (indicated above each plot in units of PFU/cell).

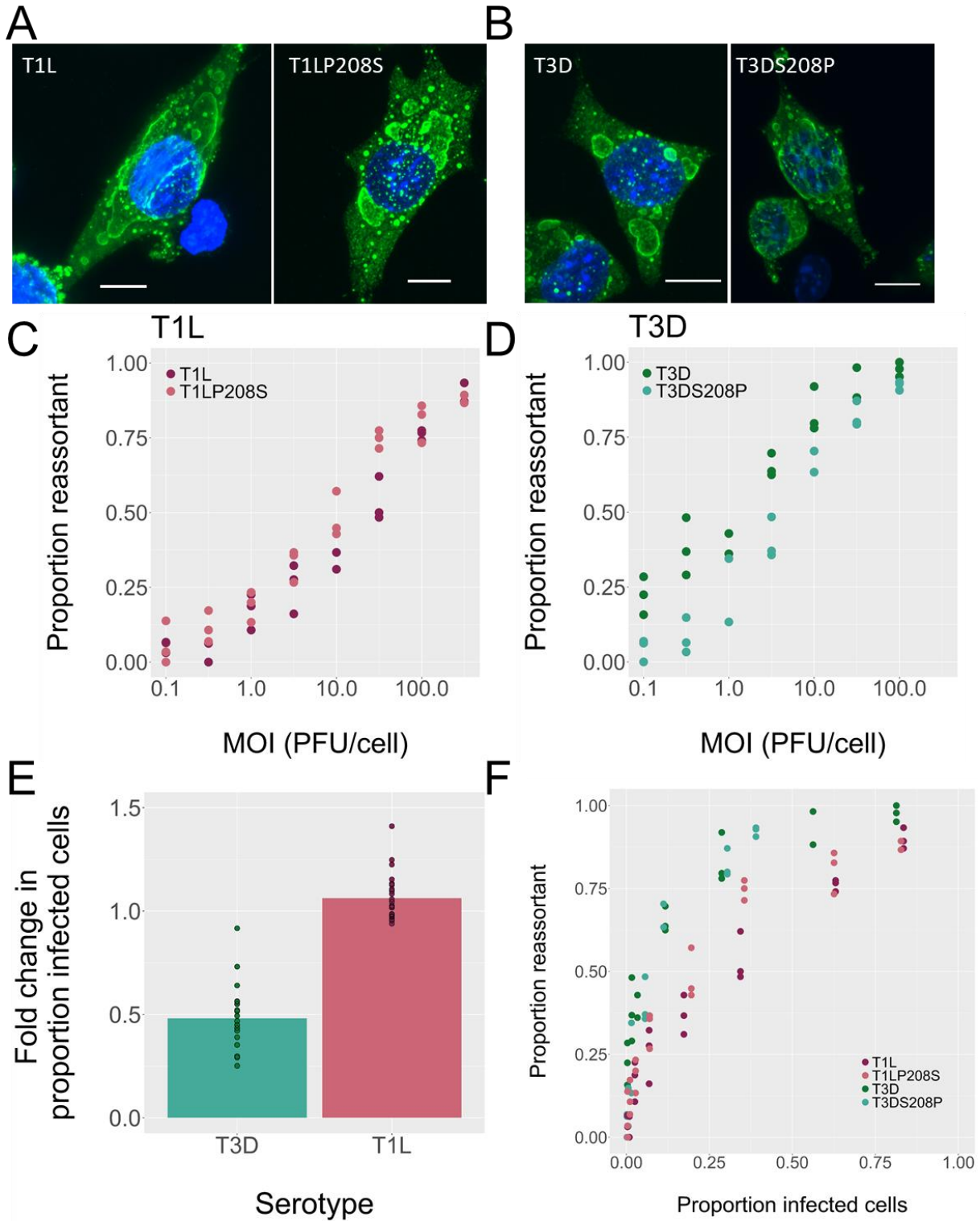


**Figure 4: Reassortment efficiency is not strongly modulated by inclusion morphology.** (A, B) The morphology of cytoplasmic inclusions formed by wild-type viruses and those with altered amino acid identities at  $\mu 2$  position 208 was characterized by confocal microscopy, staining for nuclei (blue) and viral  $\sigma$ NS protein (green). Filamentous T1L inclusions are changed to a globular morphology with the introduction of  $\mu 2$  P208S (A). The converse is observed with T3D and T3D  $\mu 2$  S208P (B). Projections from a Z stack are shown. Scale bars, 10  $\mu$ m. (C, D) Reassortment was quantified for the globular T1LP208S (C) and filamentous T3DS208P (D) viruses, and plotted together with data shown in Figure 2 for filamentous T1L and globular T3D, respectively. (E) The fold change in the proportion of cells positive for  $\sigma 3$  is plotted, comparing inoculation with mutant virus (T1LP208S and T3DS208P) to inoculation with wild-type virus (T1L and T3D) at a given MOI. Data points indicate fold change values observed at each MOI and bars show the mean across all MOIs. (F) Reassortment data from (C) and (D) are re-plotted against the proportion of cells expressing viral  $\sigma 3$  protein.

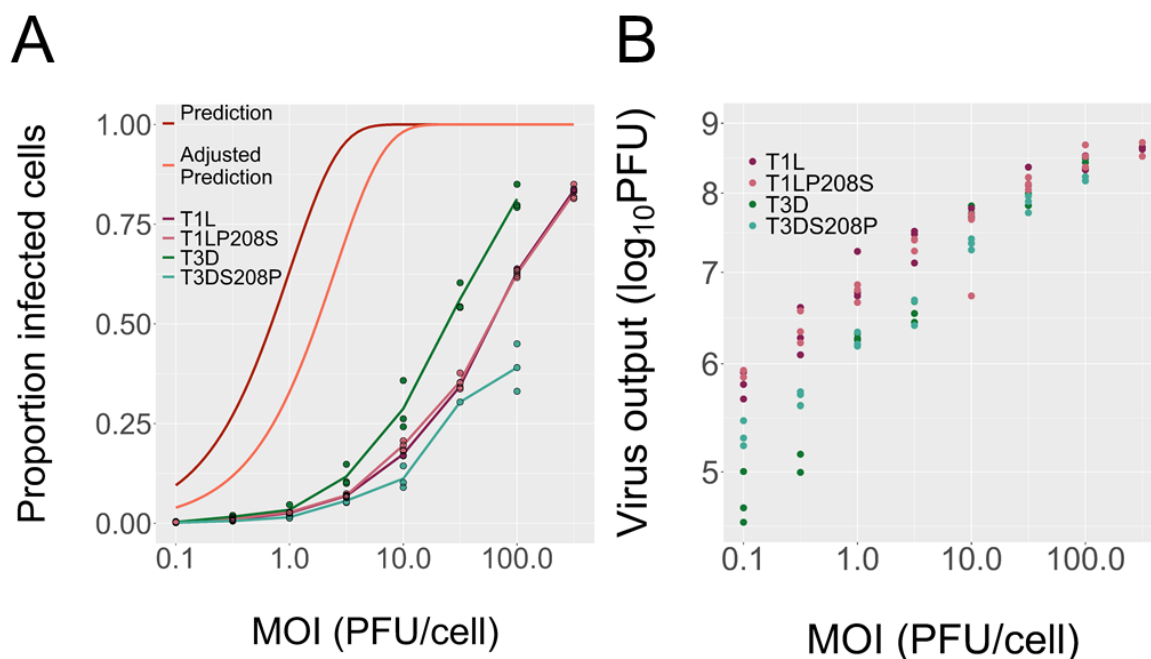


**Figure 5: Flow cytometry-based detection of reovirus-positive cells appears to under-represent levels of infection.** The infectivity of T3D, T3DS208P, T1L, and T1LP208S viruses was measured using flow cytometry targeting  $\sigma 3$ . (A) The proportion of cells expressing viral antigen was plotted against MOI. Predicted infection levels were determined based on the Poisson distribution, considering the intended MOI (Prediction) and the adjusted MOI based on the amount of inoculum virus recovered in washes (Adjusted Prediction). (B) Viral yield from *wt-var* co-infections was plotted against MOI.

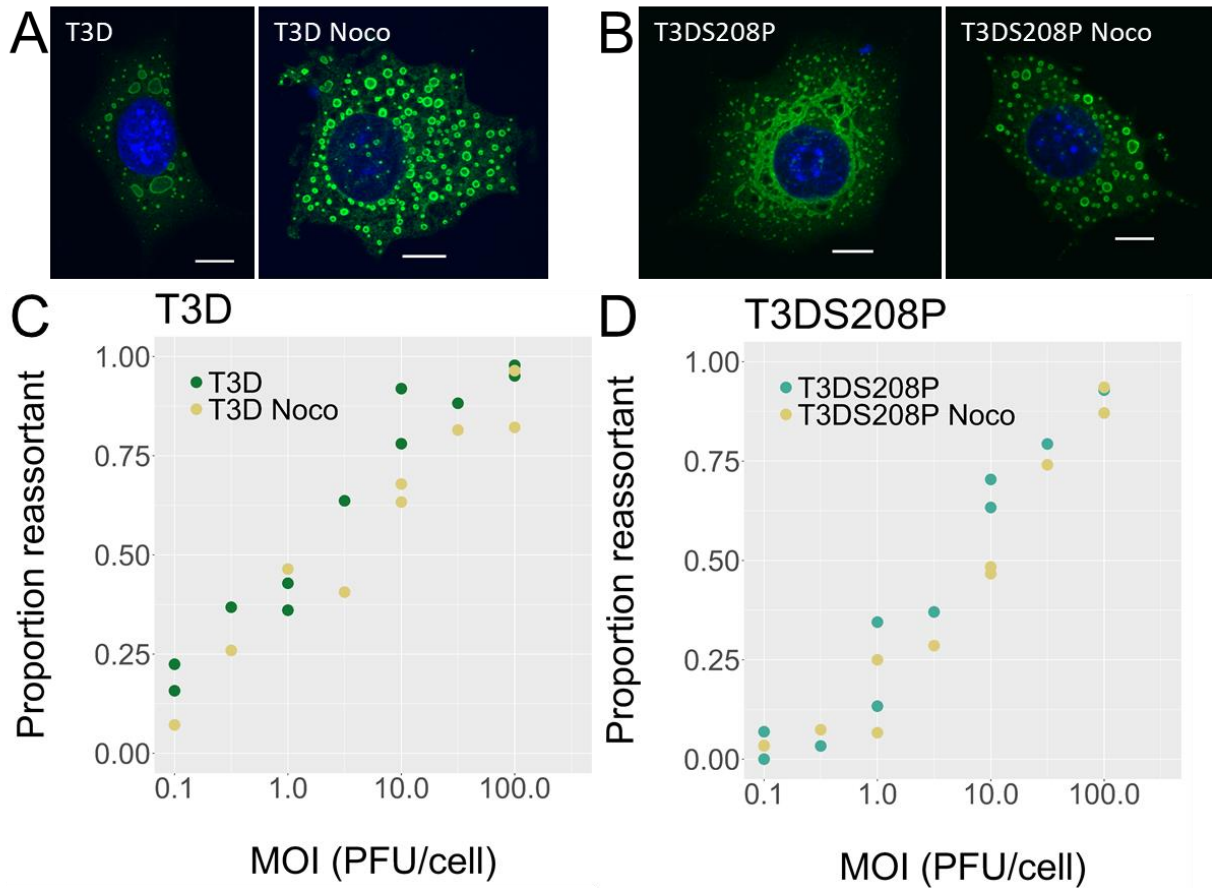


**Figure 6: Treatment of cells with nocodazole does not impact reassortment.** (A, B) Inclusion morphologies were visualized in cells treated with nocodazole and in untreated cells using confocal microscopy staining for L929 cell nuclei (blue) and viral  $\sigma$ NS protein (green). Projections from a Z-stack are shown. Scale bars, 10  $\mu$ m. (C, D) Reassortment was quantified for both T3D and T3DS208P viruses in the presence of nocodazole. These results are compared to reassortment frequencies without nocodazole, also reported in Figures 2 or 3.

## References

1. Ince WL, Gueye-Mbaye A, Bennink JR, Yewdell JW. 2013. Reassortment complements spontaneous mutation in influenza A virus NP and M1 genes to accelerate adaptation to a new host. *J Virol* 87:4330-8.
2. Simon-Loriere E, Holmes EC. 2011. Why do RNA viruses recombine? *Nat Rev Microbiol* 9:617-26.
3. Chao L. 1997. Evolution of sex and the molecular clock in RNA viruses. *Gene* 205:301-8.
4. Chao L, Tran TT, Tran TT. 1997. The advantage of sex in the RNA virus phi6. *Genetics* 147:953-9.
5. Fonville JM, Marshall N, Tao H, Steel J, Lowen AC. 2015. Influenza Virus Reassortment Is Enhanced by Semi-infectious Particles but Can Be Suppressed by Defective Interfering Particles. *PLoS Pathog* 11:e1005204.
6. Jacobs NT, Onuoha NO, Antia A, Steel J, Antia R, Lowen AC. 2019. Incomplete influenza A virus genomes occur frequently but are readily complemented during localized viral spread. *Nat Commun* 10:3526.
7. Phipps KL, Ganti K, Jacobs NT, Lee CY, Carnaccini S, White MC, Manandhar M, Pickett BE, Tan GS, Ferreri LM, Perez DR, Lowen AC. 2020. Collective interactions augment influenza A virus replication in a host-dependent manner. *Nat Microbiol* 5:1158-1169.
8. Sharpe AH, Chen LB, Fields BN. 1982. The interaction of mammalian reoviruses with the cytoskeleton of monkey kidney CV-1 cells. *Virology* 120:399-411.
9. Parker JS, Broering TJ, Kim J, Higgins DE, Nibert ML. 2002. Reovirus core protein mu2 determines the filamentous morphology of viral inclusion bodies by interacting with and stabilizing microtubules. *J Virol* 76:4483-96.
10. Broering TJ, Parker JS, Joyce PL, Kim J, Nibert ML. 2002. Mammalian reovirus nonstructural protein microNS forms large inclusions and colocalizes with reovirus microtubule-associated protein micro2 in transfected cells. *J Virol* 76:8285-97.
11. Knipe DM, Howley PM. 2013. *Fields virology*, 6th ed. Wolters Kluwer/Lippincott Williams & Wilkins Health, Philadelphia, PA.
12. Miller CL, Broering TJ, Parker JS, Arnold MM, Nibert ML. 2003. Reovirus sigma NS protein localizes to inclusions through an association requiring the mu NS amino terminus. *J Virol* 77:4566-76.
13. Broering TJ, Kim J, Miller CL, Piggott CD, Dinoso JB, Nibert ML, Parker JS. 2004. Reovirus nonstructural protein mu NS recruits viral core surface proteins and entering core particles to factory-like inclusions. *J Virol* 78:1882-92.
14. Miller CL, Arnold MM, Broering TJ, Hastings CE, Nibert ML. 2010. Localization of mammalian orthoreovirus proteins to cytoplasmic factory-like structures via nonoverlapping regions of microNS. *J Virol* 84:867-82.

15. Tenorio R, Fernandez de Castro I, Knowlton JJ, Zamora PF, Lee CH, Mainou BA, Dermody TS, Risco C. 2018. Reovirus sigmaNS and muNS Proteins Remodel the Endoplasmic Reticulum to Build Replication Neo-Organelles. *mBio* 9.
16. Fernandez de Castro I, Zamora PF, Ooms L, Fernandez JJ, Lai CM, Mainou BA, Dermody TS, Risco C. 2014. Reovirus forms neo-organelles for progeny particle assembly within reorganized cell membranes. *mBio* 5.
17. Desmet EA, Anguish LJ, Parker JS. 2014. Virus-mediated compartmentalization of the host translational machinery. *mBio* 5:e01463-14.
18. Guo Y, Parker JSL. 2021. The Paradoxes of Viral mRNA Translation during Mammalian Orthoreovirus Infection. *Viruses* 13.
19. Shah PNM, Stanifer ML, Hohn K, Engel U, Haselmann U, Bartenschlager R, Krausslich HG, Krijnse-Locker J, Boulant S. 2017. Genome packaging of reovirus is mediated by the scaffolding property of the microtubule network. *Cell Microbiol* 19.
20. Miller CL, Parker JS, Dinoso JB, Piggott CD, Perron MJ, Nibert ML. 2004. Increased ubiquitination and other covariant phenotypes attributed to a strain- and temperature-dependent defect of reovirus core protein mu2. *J Virol* 78:10291-302.
21. Eichwald C, Ackermann M, Nibert ML. 2018. The dynamics of both filamentous and globular mammalian reovirus viral factories rely on the microtubule network. *Virology* 518:77-86.
22. Bussiere LD, Choudhury P, Bellaire B, Miller CL. 2017. Characterization of a Replicating Mammalian Orthoreovirus with Tetracysteine-Tagged muNS for Live-Cell Visualization of Viral Factories. *J Virol* 91.
23. Campbell EA, Reddy V, Gray AG, Wells J, Simpson J, Skinner MA, Hawes PC, Broadbent AJ. 2020. Discrete Virus Factories Form in the Cytoplasm of Cells Coinfected with Two Replication-Competent Tagged Reporter Birnaviruses That Subsequently Coalesce over Time. *J Virol* 94.
24. Hockman MR, Phipps KL, Holmes KE, Lowen AC. 2020. A method for the unbiased quantification of reassortment in segmented viruses. *J Virol Methods* 280:113878.
25. White MC, Lowen AC. 2018. Implications of segment mismatch for influenza A virus evolution. *J Gen Virol* 99:3-16.
26. Marshall N, Priyamvada L, Ende Z, Steel J, Lowen AC. 2013. Influenza virus reassortment occurs with high frequency in the absence of segment mismatch. *PLoS Pathog* 9:e1003421.
27. Wittwer CT, Reed GH, Gundry CN, Vandersteen JG, Pryor RJ. 2003. High-resolution genotyping by amplicon melting analysis using LCGreen. *Clin Chem* 49:853-60.
28. Spandidos DA, Graham AF. 1976. Recombination between temperature-sensitive and deletion mutants of reovirus. *J Virol* 18:117-23.

29. Fields BN. 1971. Temperature-sensitive mutants of reovirus type 3 features of genetic recombination. *Virology* 46:142-8.
30. Stuart JD, Holm GH, Boehme KW. 2018. Differential Delivery of Genomic Double-Stranded RNA Causes Reovirus Strain-Specific Differences in Interferon Regulatory Factor 3 Activation. *J Virol* 92.
31. Tyler KL, Squier MK, Rodgers SE, Schneider BE, Oberhaus SM, Grdina TA, Cohen JJ, Dermody TS. 1995. Differences in the capacity of reovirus strains to induce apoptosis are determined by the viral attachment protein sigma 1. *J Virol* 69:6972-9.
32. Berger AK, Danthi P. 2013. Reovirus activates a caspase-independent cell death pathway. *mBio* 4:e00178-13.
33. Poggioli GJ, Keefer C, Connolly JL, Dermody TS, Tyler KL. 2000. Reovirus-induced G(2)/M cell cycle arrest requires sigma1s and occurs in the absence of apoptosis. *J Virol* 74:9562-70.
34. Floyd R, Sharp DG. 1978. Viral aggregation: quantitation and kinetics of the aggregation of poliovirus and reovirus. *Appl Environ Microbiol* 35:1079-83.
35. Floyd R, Sharp DG. 1978. Viral aggregation: effects of salts on the aggregation of poliovirus and reovirus at low pH. *Appl Environ Microbiol* 35:1084-94.
36. Floyd R, Sharp DG. 1977. Aggregation of poliovirus and reovirus by dilution in water. *Appl Environ Microbiol* 33:159-67.
37. Floyd R, Sharp DG. 1979. Viral aggregation: buffer effects in the aggregation of poliovirus and reovirus at low and high pH. *Appl Environ Microbiol* 38:395-401.
38. Santiana M, Ghosh S, Ho BA, Rajasekaran V, Du WL, Mutsafi Y, De Jesus-Diaz DA, Sosnovtsev SV, Levenson EA, Parra GI, Takvorian PM, Cali A, Bleck C, Vlasova AN, Saif LJ, Patton JT, Lopalco P, Corcelli A, Green KY, Altan-Bonnet N. 2018. Vesicle-Cloaked Virus Clusters Are Optimal Units for Inter-organismal Viral Transmission. *Cell Host Microbe* 24:208-220 e8.
39. Kuss SK, Best GT, Etheredge CA, Pruijssers AJ, Frierson JM, Hooper LV, Dermody TS, Pfeiffer JK. 2011. Intestinal microbiota promote enteric virus replication and systemic pathogenesis. *Science* 334:249-52.
40. Berger AK, Yi H, Kearns DB, Mainou BA. 2017. Bacteria and bacterial envelope components enhance mammalian reovirus thermostability. *PLoS Pathog* 13:e1006768.
41. Buchholz UJ, Finke S, Conzelmann KK. 1999. Generation of bovine respiratory syncytial virus (BRSV) from cDNA: BRSV NS2 is not essential for virus replication in tissue culture, and the human RSV leader region acts as a functional BRSV genome promoter. *J Virol* 73:251-9.
42. Kobayashi T, Antar AA, Boehme KW, Danthi P, Eby EA, Guglielmi KM, Holm GH,

- Johnson EM, Maginnis MS, Naik S, Skelton WB, Wetzel JD, Wilson GJ, Chappell JD, Dermody TS. 2007. A plasmid-based reverse genetics system for animal double-stranded RNA viruses. *Cell Host Microbe* 1:147-57.
43. Rodriguez Stewart RM, Berry JTL, Berger AK, Yoon SB, Hirsch AL, Guberman JA, Patel NB, Tharp GK, Bosinger SE, Mainou BA. 2019. Enhanced Killing of Triple-Negative Breast Cancer Cells by Reassortant Reovirus and Topoisomerase Inhibitors. *J Virol* 93.
44. Furlong DB, Nibert ML, Fields BN. 1988. Sigma 1 protein of mammalian reoviruses extends from the surfaces of viral particles. *J Virol* 62:246-56.
45. Virgin HWt, Bassel-Duby R, Fields BN, Tyler KL. 1988. Antibody protects against lethal infection with the neurally spreading reovirus type 3 (Dearing). *J Virol* 62:4594-604.

## Chapter IV. Summary

### Summary

The role of reassortment in viral evolution remains a subject of debate in the field. Whether reassortment is a byproduct of genome segmentation or is selected for due to adaptive advantages remains unknown. Studying reassortment frequency in diverse virus species may yield insights into its prevalence and enhance our understanding of its importance. We have developed a method with which to quantify unbiased reassortment and used that method to quantify reassortment in mammalian orthoreovirus and gain preliminary insights into potential mechanisms underlying reassortment.

### *A Method for the Unbiased Quantification of Reassortment*

Herein, I describe the development of a method for the detection of segmented virus reassortment. While assays to quantify reassortment have been reported previously, they possess pitfalls that we sought to address. Such pitfalls include the generation of progeny with variable fitness which can arise from co-infections between phylogenetically distinct parental viruses. Selection may act in these cases, resulting in (i) preferential propagation of parental genotypes leading to an under-estimation of reassortment or (ii) preferential propagation of certain reassortants, resulting in low diversity due to selection. Performing co-infections with more similar parental viruses can reduce the likelihood of selection biasing results but requires detection measures to be sufficiently sensitive to identify subtle differences.

The method detailed in Chapter II addresses common issues that are encountered when quantifying reassortment. Highly homologous parental viruses are designed such that they have equal fitness. Because the parental viruses have equivalent fitness, reassortant progeny are expected to as well, so there will be no preferential propagation present in the system. High resolution melt analysis provides a method with which to detect small variations in segments

using PCR-based methods, which can be used to identify parental segment origin. Using this approach, costly sequencing methods are not needed for detection of polymorphisms.

Thus far this approach has only been developed in the influenza A virus and mammalian orthoreovirus systems. It requires the use of reverse genetics and is therefore limited to viruses that have a reverse genetics system already in place. Flow cytometry-based quantification of infectivity is useful for quantifying infection levels at the MOIs tested, particularly when it allows for quantification of co-infected cells. Some viruses, such as reovirus, are resistant to the addition of large tags and as such cannot be detected in this manner. Therefore, detection of reovirus is limited to overall proportion of infected cells, and not the subset that are co-infected.

#### *A Theoretical Model of Reovirus Reassortment*

In Chapter III, we quantified the reassortment of two serotypes of reovirus. These serotypes differ in their tissue tropism, induction of innate immune responses, and inclusion body morphology. As a point of comparison, we developed a theoretical model to predict reassortment frequency. This model makes a number of simple assumptions. First, the model assumes that segments mix freely within co-infected cells. Under this assumption, reassortment occurs efficiently; there is no constraint acting within the cell that may reduce reassortment levels. Second, the model assumes that viruses are distributed randomly across cells, following a Poisson distribution. Third, the model assumes that the relationship between input and output is linear. That is, that the number of viruses produced by a cell scales linearly with the number of virions that entered. While differing assumptions were explored in the model, this set of conditions was the best supported by our experimental data. Below I discuss alternative dynamics that we explored in the model and which may be relevant in different viral systems, or for reovirus in different contexts (e.g. *in vivo*).

#### *Constraint on genetic mixing in co-infected cells*

The similarity of our data to the model, which assumed free segment mixing, was unexpected given the virus' utilization of inclusion bodies to house replication. These inclusion bodies could impose physical barriers to segment mixing, reducing reassortment. The similarity of our data to a model that assumes free mixing of segments refutes this hypothesis and indicates that inclusion bodies may not be constraining genetic exchange in reovirus. The T1L serotype reassorts less frequently than model predictions. There are a number of factors that differ between T1L and T3D including inclusion morphology (T1L inclusions are filamentous, similar to most other reovirus serotypes, while T3D inclusions are globular), tissue tropism (should not be a confounding factor in our experiments, since a cell line that is highly susceptible to infections with both serotypes was used), and induction of innate immune responses (T3D induces more IFN than T1L and is more sensitive to its effects (1-3)). We changed  $\mu 2$  amino acid 208 in both the T3D and T1L serotypes, which has been demonstrated to alter inclusion morphology, and tested the impact of inclusion morphology on reassortment efficiency.

Our data indicate that alteration of inclusion morphology does not impact reassortment efficiency in either T3D or T1L. We concluded that the differences between serotypes were attributable to other features of the viral life cycle that have yet to be determined. Differences in the capacities of the serotypes to induce an innate immune response, apoptosis, and cell cycle arrest may all play an as-yet unknown role in dictating reassortment efficiency. The features of T3D and T1L that cause the observed difference in reassortment are areas for ongoing study. Our research focused on uncovering potential sources of the high reassortment levels we observed.

### *Collective dispersal*

The assumption that virus is distributed at random into target cells is reasonable based on our experimental conditions: viruses were kept in conditions that did not favor aggregation

(4, 5) and plates were rocked periodically during the attachment phase to ensure viruses were distributed over the well area. In addition, our observed infection data supported this assumption. Modification of experimental conditions, such as incubation of the inoculum at low pH to encourage aggregation, could however produce other distributions that may alter reassortment results. For example, a negative binomial distribution assumes that data varies from the mean. In a virus infection model, there would be a higher proportion of cells that are uninfected and a higher proportion of cells that are multiply infected compared to a Poisson distribution. Such a distribution could be caused by viral aggregation (4-6), delivery of multiple virions to a cell via extracellular vesicle formation (7), viral attachment to bacterial cells causing multiple infection (8, 9), or viral infection of a specific subset of cells during *in vivo* infections (1).

Each of these scenarios is possible *in vivo* and viral aggregation and interaction with bacterial components have been demonstrated *in vitro* (8, 9). There is evidence that rotavirus, a member of the *Reoviridae* family, can be packaged into extracellular vesicles (7). Whether a similar phenomenon occurs in reovirus is an area of ongoing study in the field. When the possibility of overdispersion is introduced to the reassortment model, predicted reassortment increases at low MOIs due to higher rates of co-infection. Our data did not support a model incorporating overdispersion, as measured reassortment values were either equal to (T3D) or below (T1L) the model predictions. Further research focused on the impact of different virus distributions on reassortment frequency, and its occurrence *in vivo*, could yield insights into the prevalence of reassortment within an infected host.

#### *Differing Input-Output Relationships*

The relationship between viral input and output is a potential determinant of observed reassortment frequency. At low MOIs, most cells are likely to be infected by a single or very few virions. Those that are singly infected are incapable of producing reassortants. If multiply

infected cells produce more progeny, the proportion of reassortants detected may be high. More progeny viruses will be produced by cells capable of producing reassortants than those that are not.

When parameterizing the model, we explored two different possibilities for the relationship between viral input and output. The first, and simplest, was that output remained constant. In this case, each cell produced the same number of progeny virions regardless of how many parental viruses entered. This would result in equal representation of progeny from singly and multiply infected cells. However, when we investigated the relationship between viral input and output in our co-infection experiments, output increased as a function of input. This led to the second relationship we explored in our model, where output scales linearly with input. We implemented this into the model by multiplying the number of input virions by a constant that was determined based on our data. More complex relationships, such as the implementation of a point at which the number of progeny produced reaches saturation, were considered but were not well supported by our experimental data.

#### *Reovirus Reassortment: Possible Mechanisms*

Microscopy data have shown that virus-derived inclusion bodies coalesce over time (10, 11). Live cell imaging of reovirus inclusions shows that they are both dynamic and that they merge on impact with one another (11). This motion appears to be stochastic in small inclusions that have not yet formed interactions with microtubules, and its properties are an area of ongoing study in the field. It has been hypothesized that merging of inclusion bodies from different viruses within the cell is a source of segment mixing that may give rise to reassortment (10). Interestingly, addition of the microtubule depolymerizing agent nocodazole blocks reovirus inclusions from merging. In the presence of nocodazole, inclusions were observed to move close to one another but then move away without fusing (11). We sought to use this observation to test the hypothesis that inclusion coalescence is a source of genetic exchange.

Merging was not found to be critical to genetic exchange, as blocking coalescence with nocodazole did not reduce the reassortment frequency of reovirus. The source of segment exchange remains unknown. Previous efforts to visualize viral mRNAs labeled newly transcribed species and concluded that they localized to inclusion bodies (12, 13). Experiments using fluorescence *in situ* hybridization (FISH) show viral mRNAs within the cytoplasm (14). We therefore hypothesize that genetic exchange occurs via segment trafficking between inclusion bodies through the cytoplasm. Segments may exit inclusion bodies stochastically upon localization to the periphery where ribosomes and translational machinery have been detected (15, 16). Once in the cytoplasm, viral mRNA is not a substrate for RIG-I due to the presence of a 5' cap. Viral dsRNA, not ssRNA, is believed to be an activator of cellular innate immunity; cytoplasmic mRNAs are not expected to be a trigger of cytoplasmic sensors (17). Segment re-entry into inclusions may be facilitated by the viral  $\sigma$ NS single-stranded RNA binding protein, which recruits mRNAs to viral inclusions (14). As the mRNAs in our system are highly similar, mRNAs from *wt* and *var* should be recruited with equivalent efficiency, providing a source of segment mixing that may lead to reassortment. It is unknown whether  $\sigma$ NS proteins from different serotypes differ in their recognition of mRNAs, which could reduce inter-serotypic reassortment frequency. While loss of segments to the cytoplasm could reduce the efficiency of translation and packaging – which occur within inclusions (16, 18)- recruitment of mRNAs into inclusions by  $\sigma$ NS may allow for efficient replication to proceed despite segment egress from inclusions. Our data show reassortment levels that align well with predictions assuming free mixing of segments. Cytoplasmic exchange is hypothesized to be the source of the highly efficient reassortment we observed. The lower levels of reassortment observed in T1L are not explained by differences in inclusion morphology, and therefore may be a result of other features of the reovirus life cycle that we did not study. This is an additional area for further investigation.

*Reassortment in Diverse Virus Families*

Overall, the role of reassortment in viral evolution remains an interesting question. Quantification of reassortment in isolated tissue culture environments is limited, but analysis of clinical isolates and field isolates can provide insights into the prevalence of reassortment within an infected host. It was found that between 2.7% (19) and 5.4% (20) of rotavirus clinical isolates were reassortants. Observation of reassortment in this context depends on successful co-infection of a host and sufficient proliferation of a reassortant for detection. *In vivo* experiments performed between two different rotavirus strains in mice found that reassortment levels ranged from 25% at 12 hpi to 80-100% by 96 hpi (21). These results may have been shaped by the multi-cycle conditions used, which allowed for propagation of reassortants. Additionally, these rotavirus reassortment studies investigated co-infections between genetically distinct parental strains, relying on differences in segment electrophoretic mobility for the detection of reassortants. Incompatibilities between nucleic acids or proteins of distinct parental strains may further complicate results, limiting the reassortment potential or detection of certain gene constellations. It is evident that rotavirus, a member of the *Reoviridae* family, is capable of undergoing reassortment in clinical and laboratory settings. With the recent development of a rotavirus reverse genetics platform (22) it may be possible to quantify reassortment in the absence of the complicating factors noted above.

Evidence of reassortment in other segmented virus families exists but is limited. While Lassa virus, a member of the bi-segmented *Arenaviridae* family, was observed to reassort in a laboratory setting (23), phylogenetic analysis provided no evidence of reassortment among circulating strains (24). This study highlights another possible consideration of reassortment analysis: geographic distribution. While viruses may be capable of undergoing reassortment, geographic segregation of strains may prevent co-infection. In this case, reassortment would not occur due to geographic and host factors, which is likely the reason for limited phylogenetic evidence given the potential for reassortment observed in the laboratory.

Multiple reassortant isolates of infectious bursal disease virus (IBDV), a member of the *Birnaviridae* family, have been documented (25, 26) and result in modified disease severity and pathogenicity. Inclusion coalescence is hypothesized to be the source of genetic exchange within co-infected cells (10) but thus far no quantification of reassortment in a tissue culture system has been performed. Imaging of viral mRNAs using fluorescent *in situ* hybridization (FISH) showed localization to viral inclusions (10), which may indicate that coalescence is necessary for reassortment in this system.

It is clear that reassortment is possible across multiple families of segmented viruses, but that frequency varies. This may be due to factors at multiple levels, from features of the viral life cycle to population dynamics. We sought to gain insights into whether reassortment is a necessary consequence of genome segmentation, or whether there are cases in which segments are not exchanged during cellular co-infection. Compartmentalization of viral mRNAs within inclusions was hypothesized to be one such condition that would limit reassortment, but instead reovirus reassortment was observed to be similarly efficient to a model assuming free segment mixing. It is possible that reovirus does not compartmentalize its mRNAs, but that compartmentalization could be a limiting factor of reassortment in other viruses, such as IBDV.

#### *Future Avenues of Research*

The limited number of studies quantifying reassortment in a laboratory setting makes it difficult to conclude whether there are cases where segmented viruses reassort at low levels. While limitations to reassortment at the genetic and population levels are probable, evidence for such limitations at the cellular level is lacking. Our research quantifying reassortment in the reovirus system contributes to this existing knowledge and provides further evidence that reassortment is a frequent occurrence despite features that were hypothesized to impose barriers to the process. However, further investigation is needed to determine if efficient reassortment is ubiquitous, or merely a feature of the viruses that have been studied thus far.

Development of an experimental system in which reassortment levels can be controlled is desirable for direct investigation of the degree to which reassortment facilitates adaptation. The observed aggregation of reovirus may present such a system, as manipulation of co-infection levels should result in manipulation of reassortment frequency. As noted previously, collective infection mediated by aggregation, vesicle-enclosed viruses, or attachment to bacterial components is expected to increase reassortment levels by increasing levels of co-infection at low multiplicities of infection. Comparison of adaptation in a system that promotes collective infection and one that does not may yield novel insights into the role of reassortment in virus evolution. We have designed an unbiased system in which to quantify reassortment, which will be an excellent tool in these future endeavors. Furthermore, the quantification of reassortment detailed in Chapter III lays the groundwork for future studies of both the underlying mechanisms of reovirus reassortment, and the impact of its reassortment at the population level.

## References

1. Knipe DM, Howley PM. 2013. *Fields virology*, 6th ed. Wolters Kluwer/Lippincott Williams & Wilkins Health, Philadelphia, PA.
2. Sherry B, Torres J, Blum MA. 1998. Reovirus induction of and sensitivity to beta interferon in cardiac myocyte cultures correlate with induction of myocarditis and are determined by viral core proteins. *J Virol* 72:1314-23.
3. Jacobs BL, Ferguson RE. 1991. The Lang strain of reovirus serotype 1 and the Dearing strain of reovirus serotype 3 differ in their sensitivities to beta interferon. *J Virol* 65:5102-4.
4. Floyd R, Sharp DG. 1978. Viral aggregation: effects of salts on the aggregation of poliovirus and reovirus at low pH. *Appl Environ Microbiol* 35:1084-94.
5. Floyd R, Sharp DG. 1979. Viral aggregation: buffer effects in the aggregation of poliovirus and reovirus at low and high pH. *Appl Environ Microbiol* 38:395-401.
6. Floyd R, Sharp DG. 1978. Viral aggregation: quantitation and kinetics of the aggregation of poliovirus and reovirus. *Appl Environ Microbiol* 35:1079-83.
7. Santiana M, Ghosh S, Ho BA, Rajasekaran V, Du WL, Mutsafi Y, De Jesus-Diaz DA, Sosnovtsev SV, Levenson EA, Parra GI, Takvorian PM, Cali A, Bleck C, Vlasova AN, Saif LJ, Patton JT, Lopalco P, Corcelli A, Green KY, Altan-Bonnet N. 2018. Vesicle-Cloaked Virus Clusters Are Optimal Units for Inter-organismal Viral Transmission. *Cell Host Microbe* 24:208-220 e8.
8. Berger AK, Yi H, Kearns DB, Mainou BA. 2017. Bacteria and bacterial envelope components enhance mammalian reovirus thermostability. *PLoS Pathog* 13:e1006768.
9. Erickson AK, Jesudhasan PR, Mayer MJ, Narbad A, Winter SE, Pfeiffer JK. 2018. Bacteria Facilitate Enteric Virus Co-infection of Mammalian Cells and Promote Genetic Recombination. *Cell Host Microbe* 23:77-88 e5.
10. Campbell EA, Reddy V, Gray AG, Wells J, Simpson J, Skinner MA, Hawes PC, Broadbent AJ. 2020. Discrete Virus Factories Form in the Cytoplasm of Cells Coinfected with Two Replication-Competent Tagged Reporter Birnaviruses That Subsequently Coalesce over Time. *J Virol* 94.
11. Bussiere LD, Choudhury P, Bellaire B, Miller CL. 2017. Characterization of a Replicating Mammalian Orthoreovirus with Tetracycline-Tagged muNS for Live-Cell Visualization of Viral Factories. *J Virol* 91.
12. Miller CL, Arnold MM, Broering TJ, Hastings CE, Nibert ML. 2010. Localization of mammalian orthoreovirus proteins to cytoplasmic factory-like structures via nonoverlapping regions of microNS. *J Virol* 84:867-82.

13. Tenorio R, Fernandez de Castro I, Knowlton JJ, Zamora PF, Lee CH, Mainou BA, Dermody TS, Risco C. 2018. Reovirus sigmaNS and muNS Proteins Remodel the Endoplasmic Reticulum to Build Replication Neo-Organelles. *mBio* 9.
14. Lee CH, Raghunathan K, Taylor GM, French AJ, Tenorio R, Fernandez de Castro I, Risco C, Parker JSL, Dermody TS. 2021. Reovirus Nonstructural Protein sigmaNS Recruits Viral RNA to Replication Organelles. *mBio* 12:e0140821.
15. Desmet EA, Anguish LJ, Parker JS. 2014. Virus-mediated compartmentalization of the host translational machinery. *mBio* 5:e01463-14.
16. Guo Y, Parker JSL. 2021. The Paradoxes of Viral mRNA Translation during Mammalian Orthoreovirus Infection. *Viruses* 13.
17. Holm GH, Zurney J, Tumilasci V, Leveille S, Danthi P, Hiscott J, Sherry B, Dermody TS. 2007. Retinoic acid-inducible gene-I and interferon-beta promoter stimulator-1 augment proapoptotic responses following mammalian reovirus infection via interferon regulatory factor-3. *J Biol Chem* 282:21953-61.
18. Shah PNM, Stanifer ML, Hohn K, Engel U, Haselmann U, Bartenschlager R, Krausslich HG, Krijnse-Locker J, Boulant S. 2017. Genome packaging of reovirus is mediated by the scaffolding property of the microtubule network. *Cell Microbiol* 19.
19. Iturriza-Gomara M, Isherwood B, Desselberger U, Gray J. 2001. Reassortment in vivo: driving force for diversity of human rotavirus strains isolated in the United Kingdom between 1995 and 1999. *J Virol* 75:3696-705.
20. Watanabe M, Nakagomi T, Koshimura Y, Nakagomi O. 2001. Direct evidence for genome segment reassortment between concurrently-circulating human rotavirus strains. *Arch Virol* 146:557-70.
21. Gombold JL, Ramig RF. 1986. Analysis of reassortment of genome segments in mice mixedly infected with rotaviruses SA11 and RRV. *J Virol* 57:110-6.
22. Kanai Y, Komoto S, Kawagishi T, Nouda R, Nagasawa N, Onishi M, Matsuura Y, Taniguchi K, Kobayashi T. 2017. Entirely plasmid-based reverse genetics system for rotaviruses. *Proc Natl Acad Sci U S A* 114:2349-2354.
23. Lukashevich IS. 1992. Generation of reassortants between African arenaviruses. *Virology* 188:600-5.
24. Vieth S, Torda AE, Asper M, Schmitz H, Gunther S. 2004. Sequence analysis of L RNA of Lassa virus. *Virology* 318:153-68.
25. Soubies SM, Courtillon C, Briand FX, Queguiner-Leroux M, Courtois D, Amelot M, Grousson K, Morillon P, Herin JB, Etteradossi N. 2017. Identification of a European interserotypic reassortant strain of infectious bursal disease virus. *Avian Pathol* 46:19-27.
26. Kasanga CJ, Yamaguchi T, Munang'andu HM, Ohya K, Fukushi H. 2013. Genomic sequence of an infectious bursal disease virus isolate from Zambia: classical attenuated

segment B reassortment in nature with existing very virulent segment A. Arch Virol  
158:685-9.